



저작자표시-비영리-변경금지 2.0 대한민국

이용자는 아래의 조건을 따르는 경우에 한하여 자유롭게

- 이 저작물을 복제, 배포, 전송, 전시, 공연 및 방송할 수 있습니다.

다음과 같은 조건을 따라야 합니다:



저작자표시. 귀하는 원저작자를 표시하여야 합니다.



비영리. 귀하는 이 저작물을 영리 목적으로 이용할 수 없습니다.



변경금지. 귀하는 이 저작물을 개작, 변형 또는 가공할 수 없습니다.

- 귀하는, 이 저작물의 재이용이나 배포의 경우, 이 저작물에 적용된 이용허락조건을 명확하게 나타내어야 합니다.
- 저작권자로부터 별도의 허가를 받으면 이러한 조건들은 적용되지 않습니다.

저작권법에 따른 이용자의 권리는 위의 내용에 의하여 영향을 받지 않습니다.

이것은 [이용허락규약\(Legal Code\)](#)을 이해하기 쉽게 요약한 것입니다.

[Disclaimer](#)

Thesis for Master Degree

A Study of an Autonomous Underwater
Vehicle's Navigation Algorithm using an
Extended Kalman Filter



Advisor
Professor Kim, Joon-Young

August 2017

The Graduate School of Ocean Science and Technology
Korea Maritime and Ocean University

Department of Convergence Study on the Ocean Science and Technology

Kang, Hyeon-Seok

Approved by the Committee of the Ocean Science and Technology
School of Korea Maritime and Ocean University in Fulfillment of the
Requirements for the Degree of Master's in Engineering.

Dissertation Committee :

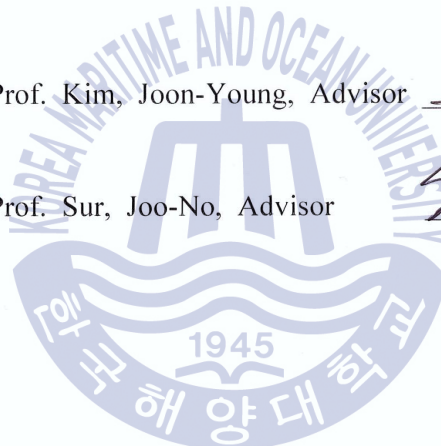
Prof. Choi, Hyeung-Sik, Chair



Prof. Kim, Joon-Young, Advisor



Prof. Sur, Joo-No, Advisor


_____

July 2017

The Graduate School of Ocean Science and Technology
Korea Maritime and Ocean University

CONTENTS

List of Tables	v
List of Figures	vi
Abstract	ix
 CHAPTER 1 INTRODUCTION	
1.1 Background	2
1.2 Objective of research	5
1.3 Organization of the thesis	9
 CHAPTER 2 GPS-AIDED NAVIGATION ALGORITHM	
2.1 Design of navigation algorithm	10
2.1.1 System model	10
2.1.2 Measurement model	11
2.1.3 Navigation algorithm using extended Kalman filter	12
 CHAPTER 3 DYNAMIC SIMULATION	
3.1 Dynamic simulation program	15
3.1.1 Block diagram of dynamic simulation	16
3.2 Dynamic model	17
3.2.1 Coordinate system	17

3.2.2 Kinematics	19
3.2.3 Kinetics	21
3.2.3.1 Rigid body dynamics	22
3.2.3.2 Restoring forces and moments	25
3.2.3.3 Equations of motion	27
3.2.3.4 Ocean currents	34
3.3 Sensor model	35
3.4 Controller	36
3.5 Scenarios	38
3.6 Simulation results	41
CHAPTER 4 FIELD TEST	
4.1 Hovering-type AUV platform	62
4.1.1 Dimensions and specifications	62
4.1.2 Boards	64
4.1.3 Sensors	66
4.1.4 Thrusters	72
4.2 Operating system	73
4.3 Experimental overview	76
4.4 Field test results	76

CHAPTER 5 CONCLUSION	84
References	86
Acknowledgement	90



List of Tables

Table 2.1 GPS-aided navigation algorithm using EKF	14
Table 3.1 The notation of SNAME for marine vehicle	19
Table 3.2 Sensor model specifications	35
Table 3.3 Scenarios list	38
Table 3.4 Colored graphs classification	41
Table 4.1 Hovering-type AUV specifications	63
Table 4.2 DVL, NavQuest 600 Micro specifications	67
Table 4.3 Magnetic compass, TCM3 specifications	68
Table 4.4 MTi AHRS specifications	69
Table 4.5 Thruster specifications	72
Table 4.6 End point position and distance comparisons	83

List of Figures

Fig. 1.1 Magnetic declination map, 2015	6
Fig. 1.2 UUV body-fixed and sensor coordinate system	7
Fig. 3.1 AUV dynamic simulation program	15
Fig. 3.2 Dynamic simulation block diagram	16
Fig. 3.3 AUV Earth-fixed and body-fixed coordinate system	18
Fig. 3.4 Rigid body dynamics reference frame	22
Fig. 3.5 Scenario 1, XY trajectory	42
Fig. 3.6 Scenario 1, Position error	43
Fig. 3.7 Scenario 1, Depth	44
Fig. 3.8 Scenario 1, Heading bias error	45
Fig. 3.9 Scenario 1, Heading angle	46
Fig. 3.10 Scenario 1, Control inputs	47
Fig. 3.11 Scenario 1, Surge velocity	48
Fig. 3.12 Scenario 2, XY trajectory	49
Fig. 3.13 Scenario 2, Position error	50
Fig. 3.14 Scenario 2, Depth	51
Fig. 3.15 Scenario 2, Heading bias error	52
Fig. 3.16 Scenario 2, Heading angle	53
Fig. 3.17 Scenario 2, Control inputs	54

Fig. 3.18 Scenario 2, Surge velocity	55
Fig. 3.19 Scenario 3, XY trajectory	56
Fig. 3.20 Scenario 3, Position error	57
Fig. 3.21 Scenario 3, Depth	58
Fig. 3.22 Scenario 3, Heading bias error	59
Fig. 3.23 Scenario 3, Heading angle	60
Fig. 3.24 Scenario 3, Control inputs	61
Fig. 3.25 Scenario 3, Surge velocity	61
Fig. 4.1 Onboard PC, mini ITX GA-H81N	64
Fig. 4.2 Edison board with breakout board	65
Fig. 4.3 GPS receiver and antenna	66
Fig. 4.4 Doppler velocity logger	67
Fig. 4.5 Tilt-compensated compass module	68
Fig. 4.6 Attitude and heading reference system	69
Fig. 4.7 Pressure sensor	70
Fig. 4.8 DIN 43650-A connector type	70
Fig. 4.9 NI USB-6009 DAQ board	71
Fig. 4.10 Tecnydyne model 280 and 300	72
Fig. 4.11 NI cDAQ-9264 DAQ board	73
Fig. 4.12 Operating system block diagram	75
Fig. 4.13 Hovering-type AUV trajectory	77

Fig. 4.14 The flag indicating whether to perform the algorithm	78
Fig. 4.15 Hovering-type AUV linear velocity	79
Fig. 4.16 The estimated heading bias error of TCM	80
Fig. 4.17 Hovering-type AUV heading angle	81
Fig. 4.18 X and Y axis distance traveled	82



A Study of an Autonomous Underwater Vehicle's Navigation Algorithm using an Extended Kalman Filter

Kang, Hyeon-Seok

Department of Convergence Study on the Ocean Science and Technology
Ocean Science and Technology School of Korea Maritime and Ocean University



Abstract

Navigation technology is vital to determine where Unmanned Underwater Vehicle (UUV) is located. This is essential to complete missions, such as submarine resource development, marine geological survey, marine ecological survey and mine clearance, and make information gathered during the mission more accurate, reliable and valuable. Dead reckoning that commonly uses Inertia Measurement Unit (IMU), Doppler Velocity Logger (DVL) and magnetic compass has position errors due to integrating acceleration and velocity. Moreover, the heading error of magnetic compass based on geodetic north includes declination and sensor noise caused by local magnetic-field effect and characteristics of sensor. This could raise the position error in the North-East-Down (NED)

coordinate system in the case of dead reckoning especially using magnetic compass, because it is based on not geodetic north, but magnetic north. This makes it difficult to implement an integrated navigation system or compare the performance of navigation algorithms, such as dead reckoning, satellite navigation using Global Positioning Systems (GPS) and terrain-aided navigation using bathymetry maps.

This thesis introduces a GPS-aided navigation algorithm to reduce errors accumulated while using dead reckoning navigation. This will help better estimate the position of UUVs while using dead reckoning in the NED coordinate system. For sensor fusion and measurement noise rejection, the navigation algorithm was designed to use an Extended Kalman Filter (EKF), which has much fewer calculations than an Unscented Kalman Filter (UKF) and a Particle Filter (PF).

This algorithm defined the heading bias error of a magnetic compass as the difference between the UUV heading angle based on geodetic north and a magnetic compass' heading measurement. The magnetic compass' heading bias error was asymptotically estimated by receiving GPS positional data when it surfaced. When the navigation algorithm estimated the magnetic compass' heading bias error, the UUV's position was displayed in the NED coordinate system, even when the UUV was submerged.

While using Matlab Simulink, an Autonomous Underwater Vehicle (AUV) dynamic simulation program was built to check the performance of the proposed navigation algorithm. The simulation program consists of a dynamic model, a sensor model, a controller and the navigation algorithm. A Naval Postgraduate School (NPS) AUV called as ARIES was used as the dynamic model because of its detailed dimensions and its precedent research containing large amounts of hydrodynamic coefficients.

Furthermore, the sensor model's characteristics were decided on according

specifications and test results of sensors currently in use. Considering the sensor characteristics, the measured values of GPS, magnetic compass, DVL, gyro and pressure sensor are artificially generated on the basis of the position, attitude and velocity of AUV in the simulation. After receiving the data, the navigation algorithm estimates the compass' heading bias error and the AUV's position allowing control of the AUV and the ability to perform way-points and heading control simulation.

The simulation incorporates three different scenarios. Two of them determine and estimate the AUV's position and heading bias error after receiving(or not) the GPS positional data. The other uses trajectory and heading bias errors similar to those in the field test which allows comparisons of the field test results.

The simulations will show that the navigation algorithm improves the accumulated positional errors of dead reckoning and the magnetic compass' heading bias errors. In the underwater driving scenario, it was confirmed that the AUV's position errors were improved. This was accomplished by the navigation algorithm examining the magnetic compass' heading bias error compared to the conventional dead reckoning method.

The GPS-aided navigation algorithm was applied to navigation system of a hovering-type AUV in order to verify the performance of the algorithm through field test. The applied algorithm estimates the position and attitude of the AUV and the heading bias error of Tilt-compensated Compass Module (TCM) based on geodetic north, by receiving the measurements of GPS, DVL, TCM and Attitude & Heading Reference System (AHRS). The monitoring and control system based on LabVIEW was implemented to provide the operator with the information about the AUV's operation. Also, the AUV operating system includes the propulsion system to perform the heading control experiment or the way-point control experiment, which can be configured by the operator. Unlike the

simulation, the application of GPS positional data and the estimation of TCM heading bias error depend on additional conditions for the efficient application of the navigation algorithm in the field test. In other words, the navigation algorithm utilizes GPS positional data to estimate the position and attitude of the AUV and the TCM heading bias error, so long as the positional information is judged to be efficient. Otherwise, the position and attitude of the AUV are estimated by dead reckoning considering the heading bias error of TCM obtained previously.

As a result, the field test verified the performance of the navigation algorithm, by checking how precisely and accurately the TCM heading bias error was estimated and comparing the position error with the conventional dead reckoning, which was not considering the heading bias error.

This thesis proposes the GPS-aided navigation algorithm for UUV. The algorithm's performance was verified by the simulation and field test. When there is no positional information provided by acoustic beacon and bathymetry map due to long-term and long-distance voyage, the navigation algorithm can be a crucial part of a UUV's navigation technology.

KEY WORDS :

Autonomous Underwater Vehicle		Extended Kalman Filter	
Navigation	Dynamic Simulation	Field Test	

CHAPTER 1 INTRODUCTION

Mankind has been making use of tools for survival which drastically developed the history of mankind. The quality of life has greatly been improved since the great revolution of civilization, also known as the Industrial Revolution. As science and technology advanced, mankind started to take an interest in the ocean's mineral, biological, energy and space resources in order to resolve the problems that mankind faced such as population increases and resources exhaustion. Several studies on Unmanned Underwater Vehicles (UUV) which have the ability to conduct development of submarine resources, exploration of submarine geology and ecology, establishment and maintenance of submarine plants were conducted especially in the United States and Europe. Recently, Monterey Bay Aquarium Research Institute (MBARI) of the U.S. conducted the exploration of submarine topography on the Gulf of California with 3685m maximum depth, and the U.S. Naval Postgraduate School (NPS) introduced some cases of using UUV for Mine Countermeasures (MCM) which was developed to overcome the limitations of divers and mammals detecting, identifying and neutralizing mines and furthermore, suggested some technical requirements for situations of searching, detecting, classifying, identifying, operating and communicating by referring to opinions of hands-on workers and experts in order to prepare for autonomous and efficient future MCM (Duane Thompson, 2012; D. Thompson, 2015; Thomas Brown, 2012). Even domestically, the need for UUVs is increasing and several industries, schools, research institutes and military are conducting studies on the core technology of UUV and some of them are already developing and operating UUVs for

research and ocean exploration (Daeyang Electric Co., 2003; Bong-huan Jun, 2007; Jae-weon Choi, 2010; Sung-min Hong, 2015; Sung-hyub Ko, 2013).

The level of technology required for UUV may vary depending on the type of UUV. UUV is mainly classified into remotely operated vehicle (ROV) which is connected to the user by cable and may be supplied with power, communicated and controlled from the outside and autonomous underwater vehicle (AUV) which requires power, navigation and control internally without connection to the outside. Particularly, AUV requires some cutting-edge technology for autonomously conducting missions.

UUV requires a wide range of technology depending on its purpose of employment and some of the core technologies for developing and employing UUVs include: hull design, propeller design, communication, energy, navigation, control, autonomous, sensor and operating system development technology (Joo-no Sur, 2010).

This thesis introduces GPS-aided navigation algorithm built through extended Kalman filter (EKF) and verifies navigation algorithm performances through dynamic simulations and field tests. This chapter includes the details of the background and the objective of the research and organization of the thesis.

1.1 Background

UUV navigation technology will provide data on the movement of UUVs which include their velocity, position and attitude. Navigation technology must provide accurate and reliable position and attitude data in order to successfully accomplish ocean navigation, submarine geology/ecological exploration, MCM, Antisubmarine Warfare (ASW) missions and UUV withdrawal. For these reasons, navigation technology is required to accurately navigate the position and attitude

of the UUV on the current map or the coordinate system.

Navigation technology can be diversely be classified, depending on the sensor and its method of application. UUV navigation technology may be classified into dead reckoning, which uses Inertia Measurement Unit (IMU) as its primary sensor and Doppler Velocity Logger (DVL) or Global Positioning System (GPS) as its secondary sensor, acoustic navigation, which uses acoustic systems such as Long Baseline (LBL), Short Baseline (SBL) and Ultrashort Baseline (USBL), geophysical navigation, which uses bathymetry map and magnetic field map, and finally complex navigation which uses two or more navigation systems (Liam Paull, 2014).

Nationally and internationally, several studies such as sensor fusion, topographic contrast, sound communication and etc., have been conducted in order to actualize the navigation system of UUVs. However, operating UUVs by installing acoustic beacons on real sea environment or using geographic features not only require additional manpower and time but also may cause failure to receive positional information. For these reasons, UUV navigation technology usually depends on dead reckoning which has the tendency to accumulate errors on the position and attitude of the vehicle due to acceleration and velocity integration.

As a study estimating the attitude of UUV by using IMU or magnetic compass, the study estimating the attitude of the body in real time by using Magnetic, Angular Rate and Gravity (MARG) sensor and designing filters, such as Complementary Filter (CF) and EKF, through transformation matrix based on not Euler angles which may cause Gimbal lock, but unit quaternion (E.R. Bachmann, 1999; Joao Luis Marins, 2001), the study estimating the attitude using Attitude and Heading Reference System (AHRS) and comparing the performances of EKF, Unscented Kalman filter (UKF) and CF through a test in water tank (Seok-Ki Jeong, 2014) and etc. were conducted.

Meanwhile, studies on estimating the position of UUVs by only using the sensors installed internally without the help of external sensors include research estimating the position by using depth gauge, DVL, magnetic compass and Strapdown Inertial Navigation System (SDINS) and establishing indirect feedback Kalman filter (Chong-moo Lee, 2003), research estimating the position by using Inertial Navigation System (INS) as primary sensor and DVL as secondary sensor (Kyung-soo Lee, 2011), research estimating the position by using inertial navigation system, echo sounder and DVL and establishing velocity filter which makes use of the thruster's rpm (Tae-suk Yoo, 2013), research estimating the position by using INS and DVL and comparing the capabilities of EKF and UKF by simulations (M. Karimi, 2013).

Recently, the U.S. Navy decided to obtain Large Displacement UUV (LDUUV) which can be employed in the Virginia Payload Module (VPM) or in the Dry Deck Shelter (DDS) of Virginia-class nuclear-powered submarine, and declared that it has plans to conduct reconnaissance-surveillance missions by deploying in the Asia Pacific regions namely the South China Sea and etc. within five years (Grace Jean, 2015). LDUUVs can be deployed in seas with diverse depths even where it is difficult for submarines to approach, and can also be employed in long time and distance compared to the existing small sized UUV. However, when the vehicle's operating hours and distance increase, cumulative position errors in dead reckoning are more likely to occur. To solve this problem, it is essential to establish an integrated navigation system which integrates various navigation systems such as satellite navigation and contrast navigation which makes use of geographic features.

Domestic researches about integrated navigation systems include:

- the research which estimates the vehicle's relative position through EKF, measuring the lineal distance from the mother ship with the aid of ultrasonic sensors, depth gauges, a digital compass and a clinometer

(Jong-hwan Lim, 2004)

- the research which limited to the plane motion on the waters and applied GPS to the navigation system in order to improve the cumulative position error of the vehicle (Won-suck Choi, 2014; Young-sik Park, 2015)

The use of GPS was less efficient for underwater navigation system due to environmental limitations.

1.2 Objective of research

A hovering-type AUV test-bed was developed to conduct studies on the core technology of UUVs and verify its capabilities through field tests. By implementing dead reckoning with DVL and Tilt-compensated Compass Module (TCM), the AUV estimates the position relative to the initial position on the coordinate system with X axis facing magnetic north. This dead reckoning may bring a cumulative position error depending on the operating time because it estimates the position by integrating velocity. Moreover, the reference coordinate system generally used is based on the geodetic north, which may cause another position error due to the difference between the reference coordinate system and the coordinate system based on magnetic north. For these reasons, dead reckoning using magnetic compass should consider declination in order to improve the position error occurred due to the difference of coordinate systems (Thor I. Fossen, 2011). To this end, it is prevalent usage to consider declination shown in **Fig. 1.1** - magnetic declination map and estimate the heading angle of the vehicle on north-east-down (NED) coordinate system through initial calibration of magnetic compass.

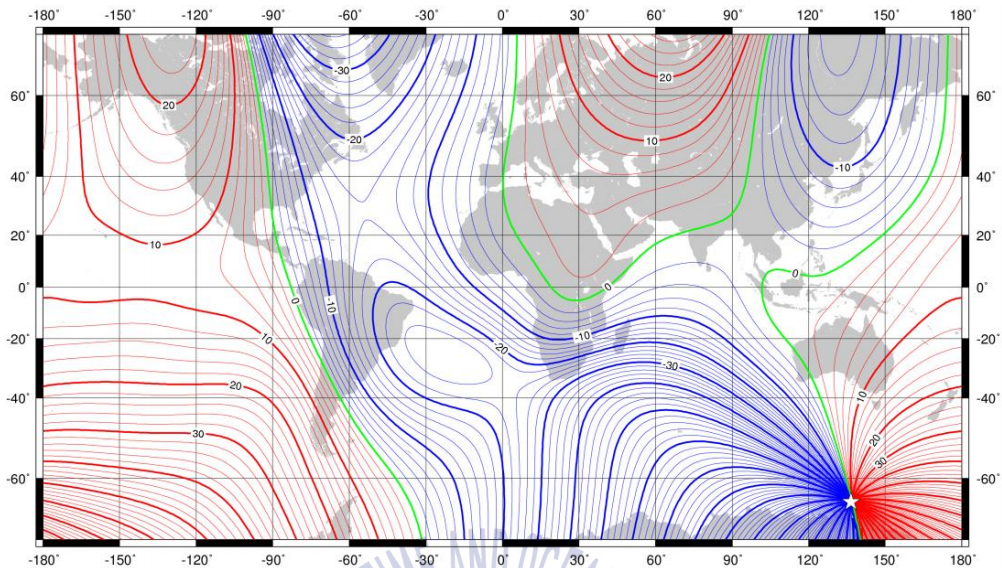


Fig. 1.1 Magnetic declination map, 2015

It is necessary to implement navigation systems considering the estimated heading angle difference of the magnetic compass to the geodetic north by moving distance and operating time, because the position of the magnetic north changes depending on time, which makes the declination change depending on time and area, and the magnetic compass is affected by the measurement noise depending on the influence of surrounding magnetic field and performance of sensors.

Prior to elaborating the difference of heading angles of magnetic compass to geodetic north, the Earth-fixed coordinate system $\{E\}$, the body-fixed coordinate system $\{B\}$, and the coordinate system of the magnetic compass installed inside are mentioned in **Fig. 1.2**.

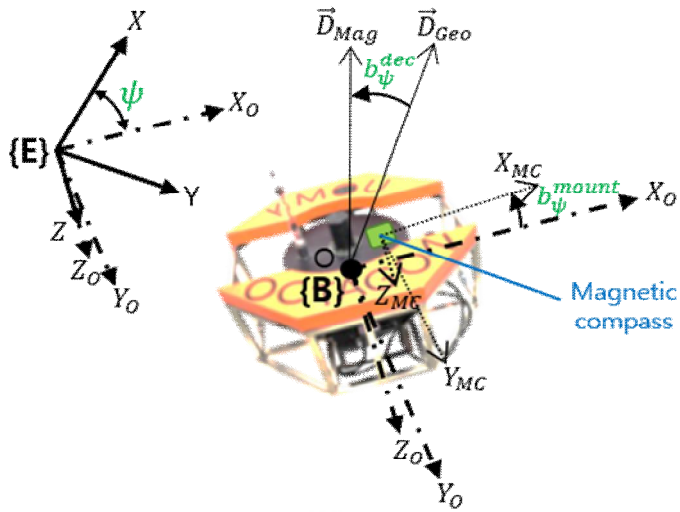


Fig. 1.2 UUV body-fixed and sensor coordinate system

Considering the nature of hovering-type AUV's movement and magnetic compasses used for this study to verify navigation algorithm, the conversion relation of the magnetic compass' coordinate system and body-fixed coordinate system can be expressed as rotation of b_{ψ}^{mount} to Z_O ($\parallel Z_{MC}$) axis. The angle b_{ψ}^{mount} represents the sensor's torsion angle based on the Z_O axis. \vec{D}_{Mag} is the direction vector from the center of body-fixed coordinate system to magnetic north. \vec{D}_{Geo} is the direction vector from the center of body-fixed coordinate system to geodetic north. The included angle of them could be marked with the declination b_{ψ}^{dec} .

The heading angle ψ of UUV to geodetic north can be expressed as equation (1.1).

$$\psi = \psi_{Mag} + b_{\psi} \quad (1.1)$$

where ψ_{Mag} is what the magnetic compass measures, which indicates the heading angle based on magnetic north, and b_ψ is the bias error of the heading angle of the magnetic compass based on geodetic north. From equation (1.2), the bias error b_ψ can be considered as the sum of magnetic declination b_ψ^{dec} , the torsion angle b_ψ^{mount} between the magnetic compass' coordinate system and the body-fixed coordinate system, and the measurement noise b_ψ^{noise} in accordance with the influence of surrounding magnetic fields and performance of sensors.

$$b_\psi = b_\psi^{dec} + b_\psi^{mount} + b_\psi^{noise} \quad (1.2)$$

The following is the main concepts of GPS-aided navigation algorithm suggested in this study. The heading angle difference of the magnetic compass to the geodetic north will be estimated together with improvement of the cumulative position error of the dead reckoning by receiving the GPS positional data when running on the water. When GPS positional data cannot be gathered, the coordinate system of dead reckoning is able to be approximated to the NED coordinate system, taking into account the initial value or the last estimated value of the heading angle difference. Thus, the position error that occurs due to the difference of the coordinate system will be improved.

1.3 Organization of the thesis

The organization of this thesis is as follows.

CHAPTER 2 GPS-AIDED NAVIGATION ALGORITHM

GPS-aided navigation algorithm established for sensor fusion and noise rejection by applying EKF will be introduced.

CHAPTER 3 DYNAMIC SIMULATION

Dynamic simulation programs implemented based on the Matlab Simulink to verify the capability of GPS-aided navigation algorithm will be introduced. The components such as dynamic model, sensor model, navigation algorithm and controller will be elaborated and the capability of navigation algorithm will be verified by conducting dynamic simulations on several scenarios.

CHAPTER 4 FIELD TEST

Navigation system with GPS-aided navigation algorithm applied on the hovering-type AUV developed on the previous research will be established and through field tests, navigation algorithm will be verified by identifying the estimation performance of position, attitude and TCM's heading bias error to geodetic north.

CHAPTER 5 CONCLUSION

Main results of this study and future plans are described.

CHAPTER 2 GPS-AIDED NAVIGATION ALGORITHM

2.1 Design of navigation algorithm

GPS-aided navigation algorithm used on this study was established through EKF. Equation of state for the continuous time as shown in equation (2.1) was drawn using the kinematic formula by assigning the required values as state vector \mathbf{x} and relevant measured values as measurement vector \mathbf{y} .

$$\begin{aligned}\dot{\mathbf{x}}(t) &= \mathbf{f}(\mathbf{x}(t)) + \mathbf{q}(t) \\ \mathbf{y}(t) &= \mathbf{h}(\mathbf{x}(t)) + \mathbf{r}(t)\end{aligned}\tag{2.1}$$

where $\mathbf{f}(\mathbf{x}(t))$ and $\mathbf{h}(\mathbf{x}(t))$ are continuous functions which represent the system and measurement model. $\mathbf{q}(t)$ and $\mathbf{r}(t)$ are covariance matrix which considered each model's noise characteristics. Also, state vector $\mathbf{x}(t)$ is the vector to be estimated by navigation algorithm and measurement vector $\mathbf{y}(t)$ is the vector for the measured value of sensors. The components represented as a matrix and vector will be further elaborated on the following.

2.1.1 System model

State vector will be assigned first prior to inducing continuous functions of

the system model. State vector $\mathbf{x}(t) \in \mathcal{R}^{7 \times 1}$ shown in equation (2.2) is composed of the position (X , Y) and the heading angle (ψ) of the vehicle on the NED coordinate system, the linear velocity (u , v) to X_O and Y_O axes and the angular velocity (r) to Z_O axis on the body-fixed coordinate system, and the heading bias error (b_ψ) of the magnetic compass assigned in the equation (1.2).

$$\mathbf{x} = [X \ Y \ \psi \ u \ v \ r \ b_\psi]^T \quad (2.2)$$

On the equation of the first derivative of the state vector, system model $\mathbf{f}(\mathbf{x})$ is expressed through kinematic relation as shown in equation (2.3).

$$\mathbf{f}(\mathbf{x}) = \begin{bmatrix} u \cos\psi - v \sin\psi \\ u \sin\psi + v \cos\psi \\ r \\ 0 \\ 0 \\ 0 \\ 0 \end{bmatrix} \quad (2.3)$$

2.1.2 Measurement model

Measurement vector will be assigned prior to inducing the continuous functions to the measurement model. Generally, measurement vector will consist of measured values which have kinematic and physical relation to the state vector. Measurement vector $\mathbf{y}(t) \in \mathcal{R}^{6 \times 1}$ is composed of measured values that have direct-indirect relations with the state vector. The components of the vector

are obtained from DVL (u_{DVL} , v_{DVL}), magnetic compass (ψ_{Mag}), gyro (r_{Gyro}) and the value (X_{GPS} , Y_{GPS}) in meters, which was transformed from the measured value of the longitude and latitude of GPS in degrees. The measurement vector is shown in equation (2.4).

$$\mathbf{y} = [u_{DVL} \quad v_{DVL} \quad \psi_{Mag} \quad r_{Gyro} \quad X_{GPS} \quad Y_{GPS}]^T \quad (2.4)$$

Measurement vector \mathbf{y} is expressed through the measurement model $\mathbf{h}(\mathbf{x})$ of equation (2.5). The measured value of the magnetic compass is represented by the heading angle of the UUV to geodetic north and the heading angle error b_ψ of magnetic compass considering the equation (1.1).

$$\mathbf{h}(\mathbf{x}) = \begin{bmatrix} u \\ v \\ \psi - b_\psi \\ r \\ X \\ Y \end{bmatrix} \quad (2.5)$$

2.1.3 Navigation algorithm using extended Kalman filter

The operation process of GPS-aided navigation algorithm using EKF on this study is shown in **Table 2.1**. The input values include the state vector $\hat{\mathbf{x}}_{k-1}$ and error covariance matrix \mathbf{P}_{k-1} estimated on the previous loop, and sensor measurement vector \mathbf{y}_k . Predicted value of the state vector will be obtained by calculating ①-④ according to the system model of equation (2.3) and integrating with ⑤. In ⑥, linearization of certain sections will take place by

partial differentiation of nonlinear function $f(x)$ and $h(x)$. In ⑦, state transition matrix Φ will be obtained by discretizing the linearized system model A_{jacob} . In ⑧, predicted value P_k^- of error covariance matrix will be obtained. It will be applied to ⑨ to calculate gain matrix K_k of EKF. Finally in ⑩-⑪, state vector and error covariance matrix will be estimated using the gain matrix of EKF.

Henceforth, the operations of the simulation's dynamic model and the hovering-type AUV platform are based on the position and attitude, which were estimated by the navigation algorithm.



Table 2.1 GPS-aided navigation algorithm using EKF

Algorithm: Navigation ($\hat{\mathbf{x}}_{k-1}$, \mathbf{P}_{k-1} , \mathbf{y}_k)

$$\textcircled{1} \quad \dot{X} = \hat{x}_{k-1|u} \cos(\hat{x}_{k-1|\psi}) - \hat{x}_{k-1|v} \sin(\hat{x}_{k-1|\psi})$$

$$\textcircled{2} \quad \dot{Y} = \hat{x}_{k-1|u} \sin(\hat{x}_{k-1|\psi}) + \hat{x}_{k-1|v} \cos(\hat{x}_{k-1|\psi})$$

$$\textcircled{3} \quad \dot{\psi} = \hat{x}_{k-1|r}$$

$$\textcircled{4} \quad \dot{u} = 0, \quad \dot{v} = 0, \quad \dot{r} = 0, \quad \dot{b}_\psi = 0$$

$$\textcircled{5} \quad \hat{\mathbf{x}}_k^- = \begin{bmatrix} \hat{x}_{k-1|X} + \dot{X}\Delta t \\ \hat{x}_{k-1|Y} + \dot{Y}\Delta t \\ \hat{x}_{k-1|\psi} + \dot{\psi}\Delta t \\ \hat{x}_{k-1|u} + \dot{u}\Delta t \\ \hat{x}_{k-1|v} + \dot{v}\Delta t \\ \hat{x}_{k-1|r} + \dot{r}\Delta t \\ \hat{x}_{k-1|b_\psi} + \dot{b}_\psi\Delta t \end{bmatrix}$$

$$\textcircled{6} \quad \mathbf{A}_{jacob} \equiv \left. \frac{\partial \mathbf{f}}{\partial \mathbf{x}} \right|_{\hat{\mathbf{x}}_{k-1}}, \quad \mathbf{H} \equiv \left. \frac{\partial \mathbf{h}}{\partial \mathbf{x}} \right|_{\hat{\mathbf{x}}_k^-}$$

$$\textcircled{7} \quad \Phi = \mathbf{I} + \mathbf{A}_{jacob}\Delta t$$

$$\textcircled{8} \quad \mathbf{P}_k^- = \Phi \mathbf{P}_{k-1} \Phi^T + \mathbf{Q}$$

$$\textcircled{9} \quad \mathbf{K}_k = \mathbf{P}_k^- \mathbf{H}^T (\mathbf{H} \mathbf{P}_k^- \mathbf{H}^T + \mathbf{R})^{-1}$$

$$\textcircled{10} \quad \hat{\mathbf{x}}_k = \hat{\mathbf{x}}_k^- + \mathbf{K}_k (\mathbf{y}_k - \mathbf{h}(\hat{\mathbf{x}}_k^-))$$

$$\textcircled{11} \quad \mathbf{P}_k = \mathbf{P}_k^- - \mathbf{K}_k \mathbf{H} \mathbf{P}_k^-$$

return $\hat{\mathbf{x}}_k$, \mathbf{P}_k

CHAPTER 3 DYNAMIC SIMULATION

3.1 Dynamic simulation program

Dynamic simulation program based on Matlab Simulink was implemented as shown in **Fig. 3.1** to verify the capability of the GPS-aided navigation algorithm suggested in this study.

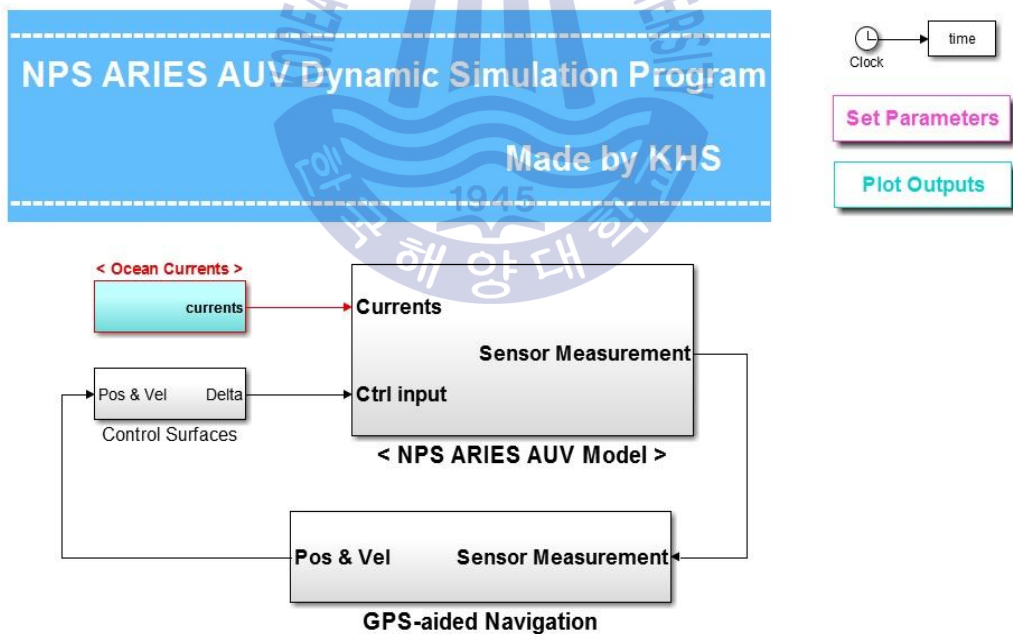


Fig. 3.1 AUV dynamic simulation program

3.1.1 Block diagram of dynamic simulation

Dynamic simulation is conducted in a similar way with the data flow of actual AUV as shown in the block diagram in **Fig. 3.2**. Depending on the flow of data, the simulation program may be classified into dynamic model of AUV, which is expressed as 6-DOF nonlinear dynamic equation, sensor model, navigation system applied with GPS-aided navigation algorithm and control system.

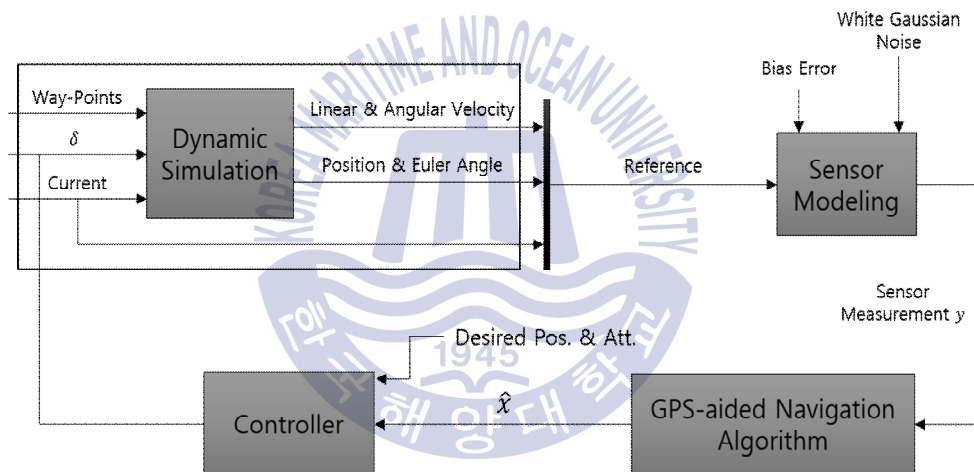


Fig. 3.2 Dynamic simulation block diagram

In order to verify the capability of the navigation algorithm, heading angle will be controlled for the AUV model to move straightforward or following several way-points that were assigned initially. The way-point control simulation will be performed to travel to each way-point, by following the Line Of Sight (LOS) method. AUV model will run by the influence of assigned current.

The values relevant to the movement of AUV model are obtained by the 6-DOF dynamic equations, and they will be defined as reference values. White

gaussian noise and bias error considering the characteristics of sensors will be added to generate output values of sensors. Some of those values will form the measurement vector \mathbf{y} of navigation algorithm. Through the measurement vector, the GPS-aided navigation algorithm will estimate the state vector including the AUV model's position, attitude and magnetic compass' heading bias error to geodetic north. Henceforth, the control system will control the propeller, steering rudder and fin in order that the estimated state vector $\hat{\mathbf{x}}$ will be similar with the desired position and attitude.

3.2 Dynamic model

Since various hydrodynamic coefficients were calculated through previously conducted research, the NPS ARIES AUV was selected as the dynamic model of this simulation program.

3.2.1 Coordinate system

Prior to expression of the AUV's movement in dynamic equations, Earth-fixed coordinate system $\{E\}$ which is based on geodetic north and body-fixed coordinate system $\{B\}$ with the point fixed on the center of buoyancy of an AUV are shown in **Fig. 3.3**. The Earth-fixed coordinate system designates the positive direction of X axis as the direction to the geodetic north, namely positive latitude, and the positive direction of Y axis as the direction of positive longitude. The body-fixed coordinate system designates the positive direction of X_O axis as the ahead, the positive direction of Y_O axis as the starboard and the positive direction of Z_O axis as the bottom.

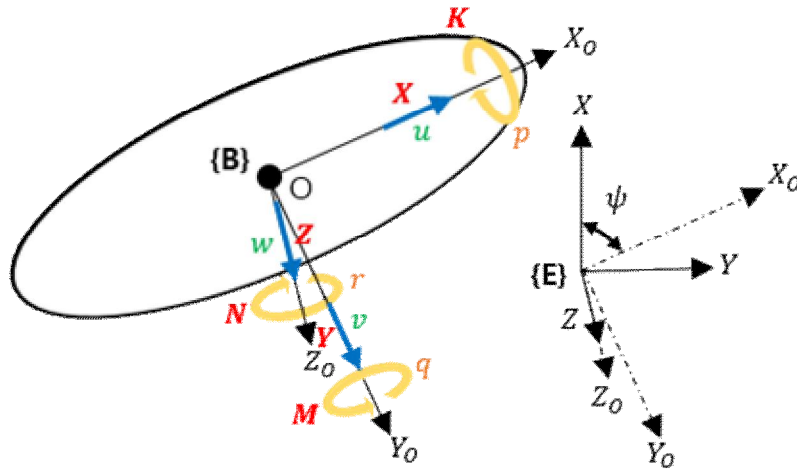


Fig. 3.3 AUV Earth-fixed and body-fixed coordinate system

The variables, which are required for expression of the AUV's motion by using 6-DOF dynamic equations, are defined as shown in **Table 3.1** in accordance with the notation of SNAME (SNAME, 1950). Force and moment are applied on each axis of the body-fixed coordinate system. The linear and angular velocity variables occurred as a result of those will be defined in order to elaborate the translational and rotational motion of the body-fixed coordinate system. Also, translational and rotational motion relative to the Earth-fixed coordinate system will be elaborated by defining the position and attitude variables of each axis in the Earth-fixed coordinate system.

The research of dynamic modeling of AUVs is mainly classified into kinetics, which considers the geometrical aspects, and kinematics, which considers force and moment. Next section will discuss dynamic modeling, as elaborating on the kinetic and kinematic analysis of the dynamic model.

Table 3.1 The notation of SNAME for marine vehicle

Translational motion	Linear velocity	Position	Forces
Surge	u	x	X
Sway	v	y	Y
Heave	w	z	Z
Rotational motion	Angular velocity	Euler Angle	Moments
Roll	p	ϕ	K
Pitch	q	θ	M
Yaw	r	ψ	N

3.2.2 Kinematics

Generally, the movement of AUVs can be expressed in the body-fixed coordinate system and Earth-fixed coordinate system. This study expresses the movement of AUVs in the NED coordinate system which is one of the Earth-fixed coordinate systems. AUVs movement variables expressed in body-fixed coordinate systems and NED coordinate systems could be interconverted through the transformation matrix \mathbf{J}_Θ shown in equation (3.1).

$$\dot{\boldsymbol{\eta}} = \mathbf{J}_\Theta(\boldsymbol{\eta})\boldsymbol{\nu} ; \quad \begin{bmatrix} \dot{\mathbf{p}}_{b/n}^n \\ \dot{\boldsymbol{\Theta}}_{nb} \end{bmatrix} = \begin{bmatrix} \mathbf{R}_b^n(\boldsymbol{\Theta}_{nb}) & \mathbf{0}_{3 \times 3} \\ \mathbf{0}_{3 \times 3} & \mathbf{T}_\Theta(\boldsymbol{\Theta}_{nb}) \end{bmatrix} \begin{bmatrix} \mathbf{v}_{b/n}^b \\ \boldsymbol{\omega}_{b/n}^b \end{bmatrix} \quad (3.1)$$

Matrix \mathbf{J}_Θ represents the transformation matrix between a body-fixed coordinate system and the NED coordinate system. Superscript n or b represents

that the values are expressed in the NED coordinate system or body-fixed coordinate system. The vector for variables, which represents the position, attitude, linear velocity and angular velocity in each coordinate system, is shown in equation (3.2).

$$\boldsymbol{\eta} = \begin{bmatrix} \mathbf{p}_{b/n}^n \\ \boldsymbol{\Theta}_{nb} \end{bmatrix} ; \quad \mathbf{p}_{b/n}^n = \begin{bmatrix} x \\ y \\ z \end{bmatrix} ; \quad \boldsymbol{\Theta}_{nb} = \begin{bmatrix} \phi \\ \theta \\ \psi \end{bmatrix} \quad (3.2)$$

$$\boldsymbol{\nu} = \begin{bmatrix} \mathbf{v}_{b/n}^n \\ \boldsymbol{\omega}_{b/n}^b \end{bmatrix} ; \quad \mathbf{v}_{b/n}^b = \begin{bmatrix} u \\ v \\ w \end{bmatrix} ; \quad \boldsymbol{\omega}_{b/n}^b = \begin{bmatrix} p \\ q \\ r \end{bmatrix}$$

where $\mathbf{p}_{b/n}^n$ and $\boldsymbol{\Theta}_{nb}$ are vectors which represent the position and attitude of the AUV in the NED coordinate system respectively. $\mathbf{v}_{b/n}^b$ and $\boldsymbol{\omega}_{b/n}^b$ are vectors which represent the linear velocity and angular velocity of an AUV in the body-fixed coordinate system respectively.

The transformation matrix $\mathbf{J}_{\boldsymbol{\Theta}}$ between the two coordinate systems is composed of a transformation matrix \mathbf{R}_b^n and $\mathbf{T}_{\boldsymbol{\Theta}}$. The transformation matrix \mathbf{R}_b^n which is used to convert linear velocity $\mathbf{v}_{b/n}^b$ in the body-fixed coordinate system into linear velocity $\dot{\mathbf{p}}_{b/n}^n$ in the NED coordinate system is expressed as shown in equation (3.3).

$$\mathbf{R}_b^n(\boldsymbol{\Theta}_{nb}) = \begin{bmatrix} \cos \psi \cos \theta & \cos \psi \sin \theta \sin \phi - \sin \psi \cos \phi \\ \sin \psi \cos \theta & \cos \psi \cos \phi + \sin \psi \sin \theta \sin \phi \\ -\sin \theta & \cos \theta \sin \phi \\ & \sin \psi \sin \phi + \cos \psi \sin \theta \cos \phi \\ & \sin \psi \sin \theta \cos \phi - \cos \psi \sin \phi \\ & \cos \theta \cos \phi \end{bmatrix} \quad (3.3)$$

Also, transformation matrix T_{Θ} which is used to convert the angular velocity $\omega_{b/n}^b$ in the body-fixed system into angular velocity $\dot{\Theta}_{nb}$ in the NED coordinate system can be expressed as equation (3.4).

$$T_{\Theta}(\Theta_{nb}) = \begin{bmatrix} 1 & \tan \theta \sin \phi & \tan \theta \cos \phi \\ 0 & \cos \phi & -\sin \phi \\ 0 & \sin \phi / \cos \theta & \cos \phi / \cos \theta \end{bmatrix} \quad (3.4)$$

Transformation matrix T_{Θ} will have a singularity when $\theta = \pm 90^\circ$ in the equation (3.4), making it impossible to convert. When the model has a chance of having a singularity, considering the movement of the model, unit quaternion method can be used to construct the transformation matrix between the two coordinate systems. However, since the chances of singularity are unlikely due to the model's characteristics, the transformation matrix shown in the equation (3.4) will be used.

3.2.3 Kinetics

Rigid body dynamics, hydrodynamics and hydrostatics must be considered in order to induce the dynamic equations of AUV (Fossen, 1994). The dynamic equations of the model applied to the simulation program will be described after summarizing the rigid body dynamics, restoring forces and moments.

3.2.3.1 Rigid body dynamics

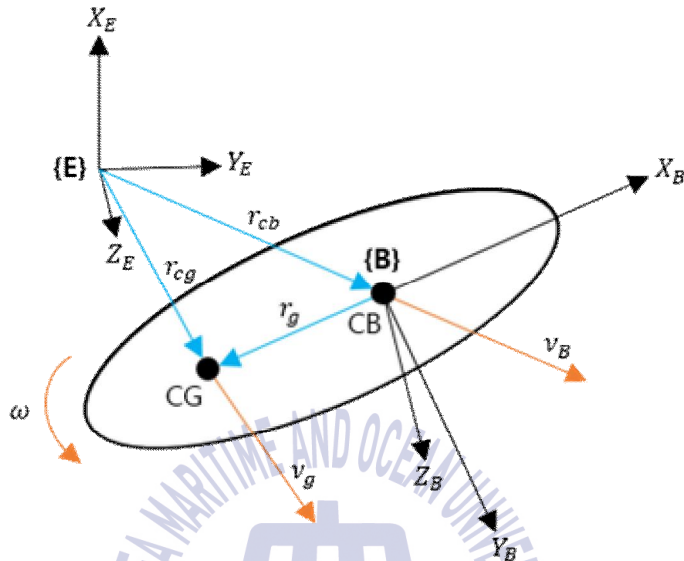


Fig. 3.4 Rigid body dynamics reference frame

The dynamic equations of the rigid body moving in 6-DOF can be obtained by assuming an AUV as one rigid body as shown in Fig. 3.4. Earth-fixed coordinate system $\{E\}$ is expressed as coordinate system $X_E Y_E Z_E$ and body-fixed coordinate system $\{B\}$ with the origin on the body's center of buoyancy CB is expressed as coordinate system $X_B Y_B Z_B$. CG and CB are the center of gravity and center of buoyancy of the rigid body respectively, and the vectors to CG and CB from the origin in the Earth-fixed coordinate system are expressed as r_{cg} and r_{cb} respectively. The rigid body moves with linear velocity v_B and angular velocity ω .

The dynamic equations of AUV assumed as one rigid body will be induced through the Newton-Euler's formula based on Newton's second law, the law of acceleration. The dynamic equations for translational motion and rotational

motion in the body-fixed coordinate system can be expressed as shown in equation (3.5) and (3.6) respectively, using vectors.

$$m \left[\dot{\mathbf{v}}_{b/n}^b + \dot{\boldsymbol{\omega}}_{b/n}^b \times \mathbf{r}_g^b + \boldsymbol{\omega}_{b/n}^b \times \mathbf{v}_{b/n}^b + \boldsymbol{\omega}_{b/n}^b \times (\boldsymbol{\omega}_{b/n}^b \times \mathbf{r}_g^b) \right] = \mathbf{f}_b^b \quad (3.5)$$

$$\mathbf{I}_b \dot{\boldsymbol{\omega}}_{b/n}^b + \boldsymbol{\omega}_{b/n}^b \times \mathbf{I}_b \boldsymbol{\omega}_{b/n}^b + m \mathbf{r}_g^b \times (\dot{\mathbf{v}}_{b/n}^b + \boldsymbol{\omega}_{b/n}^b \times \mathbf{v}_{b/n}^b) = \mathbf{m}_b^b \quad (3.6)$$

where m represents the mass of the rigid body, while \mathbf{f}_b^b and \mathbf{m}_b^b respectively represent the force and moment working on the origin of the body-fixed coordinate system, which are expressed as the equation (3.7).

$$\mathbf{f}_b^b = \begin{bmatrix} X \\ Y \\ Z \end{bmatrix} ; \quad \mathbf{m}_b^b = \begin{bmatrix} K \\ M \\ N \end{bmatrix} \quad (3.7)$$

Also, \mathbf{r}_g^b represents the vector from the center of buoyancy CB to the center of gravity CG , which are expressed in the body-fixed coordinate system, while matrix \mathbf{I}_b represents the inertia matrix for the center of buoyancy as shown in equation (3.8).

$$\mathbf{r}_g^b = \begin{bmatrix} x_g \\ y_g \\ z_g \end{bmatrix} ; \quad \mathbf{I}_b = \begin{bmatrix} I_x & -I_{xy} & -I_{xz} \\ -I_{yx} & I_y & -I_{yz} \\ -I_{zx} & -I_{zy} & I_z \end{bmatrix} \quad (3.8)$$

Rigid body dynamics in the 3-dimensional space expressed as the equation

(3.5) and (3.6) can be reorganized as shown in equation (3.9).

$$\mathbf{M}_{RB}\dot{\boldsymbol{\nu}} + \mathbf{C}_{RB}(\boldsymbol{\nu})\boldsymbol{\nu} = \boldsymbol{\tau}_{RB} \quad (3.9)$$

where $\boldsymbol{\nu}$ is the vector which represents the linear velocity and angular velocity of AUV in the body-fixed coordinate system while $\boldsymbol{\tau}_{RB} = [X \ Y \ Z \ K \ M \ N]^T$ is the vector which represents the force and moment that work on AUV in body-fixed coordinate system. \mathbf{M}_{RB} is the inertia matrix of the rigid body while \mathbf{C}_{RB} is the matrix for the Coriolis effect and the centripetal force due to the rotation of the earth, which can be expressed as equation (3.10) and (3.11) respectively.

$$\mathbf{M}_{RB} = \begin{bmatrix} m\mathbf{I}_{3 \times 3} & -m\mathbf{S}(\mathbf{r}_g^b) \\ m\mathbf{S}(\mathbf{r}_g^b) & \mathbf{I}_b \end{bmatrix} = \begin{bmatrix} m & 0 & 0 & 0 & mz_g & -my_g \\ 0 & m & 0 & -mz_g & 0 & mx_g \\ 0 & 0 & m & my_g & -mx_g & 0 \\ 0 & -mz_g & my_g & I_x & -I_{xy} & -I_{xz} \\ mz_g & 0 & -mx_g & -I_{yx} & I_y & -I_{yz} \\ -my_g & mx_g & 0 & -I_{zx} & -I_{zy} & I_z \end{bmatrix} \quad (3.10)$$

$$\mathbf{C}_{RB} = \begin{bmatrix} 0 & 0 & 0 \\ 0 & 0 & 0 \\ 0 & 0 & 0 \\ -m(y_gq + z_gr) & m(y_gp + w) & m(z_gp - v) \\ m(x_gq - w) & -m(z_gr + x_gp) & m(z_gq + u) \\ m(x_gr + v) & m(y_gr - u) & -m(x_gp + y_gq) \\ m(y_gq + z_gr) & -m(x_gq - w) & -m(x_gr + v) \\ -m(y_gp + w) & m(z_gr + x_gp) & -m(y_gr - u) \\ -m(z_gp - v) & -m(z_gq + u) & m(x_gp + y_gq) \\ 0 & -I_{yz}q - I_{xz}p + I_zr & I_{yz}r + I_{xy}p - I_yq \\ I_{yz}q + I_{xz}p - I_zr & 0 & -I_{xz}r - I_{xy}q + I_xp \\ -I_{yz}r - I_{xy}p + I_yq & I_{xz}r + I_{xy}q - I_xp & 0 \end{bmatrix} \quad (3.11)$$

where I_{ij} represents the moments of inertia about each axes or the products of inertia of the AUV. Since $\mathbf{S}(\mathbf{r}_g^b)$ is a skew-symmetric matrix expressed as equation (3.12), $\mathbf{S} = -\mathbf{S}^T$ is satisfied and the diagonal elements of the matrix are 0.

$$\mathbf{S}(\mathbf{r}_g^b) = \begin{bmatrix} 0 & -z_g & y_g \\ z_g & 0 & -x_g \\ -y_g & x_g & 0 \end{bmatrix} \quad (3.12)$$

3.2.3.2 Restoring forces and moments

Gravity and buoyancy generate restoring forces because the two forces are always working regardless of the movement of the AUV. Gravity \mathbf{f}_g^b works on the center of gravity CG , which is expressed as vector \mathbf{r}_g^b in the body-fixed coordinate system, and buoyancy \mathbf{f}_b^b works on the center of buoyancy CB , which is expressed as vector \mathbf{r}_b^b of equation (3.13).

$$\mathbf{r}_b^b = \begin{bmatrix} x_b \\ y_b \\ z_b \end{bmatrix} \quad (3.13)$$

Equation (3.14) shows the AUV's weight W and buoyancy B which works on the body.

$$W = mg ; \quad B = \rho g \nabla \quad (3.14)$$

where g is the gravitational acceleration of the earth and ρ is the density of the liquid that the object is immersed, while ∇ is the immersed volume of the object. Also, gravity and buoyancy work on the Z axis in the Earth-fixed coordinate system and can be expressed as equation (3.15).

$$\mathbf{f}_g^n = \begin{bmatrix} 0 \\ 0 \\ W \end{bmatrix} ; \quad \mathbf{f}_b^n = - \begin{bmatrix} 0 \\ 0 \\ B \end{bmatrix} \quad (3.15)$$

Through transformation matrix using Euler angles, gravity and buoyancy in Earth-fixed coordinate system can be expressed in body-fixed coordinate system as equation (3.16) and (3.17).

$$\mathbf{f}_g^b = \mathbf{R}_b^n(\boldsymbol{\Theta}_{nb})^{-1} \mathbf{f}_g^n \quad (3.16)$$

$$\mathbf{f}_b^b = \mathbf{R}_b^n(\boldsymbol{\Theta}_{nb})^{-1} \mathbf{f}_b^n \quad (3.17)$$

Force and moment caused by the restoring force of AUV can be expressed as gravity and buoyancy working on AUV as shown in equation (3.18).

$$\mathbf{g}(\boldsymbol{\eta}) = - \begin{bmatrix} \mathbf{f}_g^b + \mathbf{f}_b^b \\ \mathbf{r}_g^b \times \mathbf{f}_g^b + \mathbf{r}_b^b \times \mathbf{f}_b^b \end{bmatrix} = - \begin{bmatrix} \mathbf{R}_b^n(\boldsymbol{\Theta}_{nb})^{-1}(\mathbf{f}_g^n + \mathbf{f}_b^n) \\ \mathbf{r}_g^b \times \mathbf{R}_b^n(\boldsymbol{\Theta}_{nb})^{-1} \mathbf{f}_g^n + \mathbf{r}_b^b \times \mathbf{R}_b^n(\boldsymbol{\Theta}_{nb})^{-1} \mathbf{f}_b^n \end{bmatrix} \quad (3.18)$$

Vector for the restoring force and moment of AUV can be expressed as shown in equation (3.19), by substituting the vectors mentioned previously in the equation (3.18).

$$\mathbf{g}(\boldsymbol{\eta}) = \begin{bmatrix} (W-B) \sin \theta \\ -(W-B) \cos \theta \sin \phi \\ -(W-B) \cos \theta \cos \phi \\ -(y_g W - y_b B) \cos \theta \cos \phi + (z_g W - z_b B) \cos \theta \sin \phi \\ (z_g W - z_b B) \sin \theta + (x_g W - x_b B) \cos \theta \cos \phi \\ -(x_g W - x_b B) \cos \theta \sin \phi - (y_g W - y_b B) \sin \theta \end{bmatrix} \quad (3.19)$$

3.2.3.3 Equations of motion

The dynamic simulation program in this study uses the NPS ARIES AUV whose specification, dimension and a number of hydrodynamic coefficients were known through precedent study. The model's 6-DOF dynamic equations can be arranged as shown in equation (3.20) using matrices and vectors.

$$\mathbf{M}\dot{\boldsymbol{\nu}} + \mathbf{C}(\boldsymbol{\nu})\boldsymbol{\nu} + \mathbf{D}(\boldsymbol{\nu})\boldsymbol{\nu} + \mathbf{g}(\boldsymbol{\eta}) = \boldsymbol{\tau} \quad (3.20)$$

where \mathbf{M} is the inertia matrix of the system, \mathbf{C} the matrix of Coriolis-centripetal force, \mathbf{D} the damping matrix, \mathbf{g} restoring force and moment vector due to gravity and buoyancy, and $\boldsymbol{\tau}$ is for the force and moment vector working on the AUV due to external forces. The equation of these is expressed as follows, respectively.

$$\mathbf{M} = \mathbf{M}_{RB} + \mathbf{M}_A \quad (3.21)$$

$$C = C_{RB} + C_A \quad (3.22)$$

$$D = D_P + D_S + D_W + D_M \quad (3.23)$$

M_A in the equation (3.21) is the inertia matrix for the mass exerted on AUV due to the surrounding fluid, and C_A in the equation (3.22) is the matrix considering the Coriolis effect and centripetal force for the added mass. D_P in the equation (3.23) is for radiation-induced potential damping due to forced body oscillations caused by the surface wave, D_S for linear skin friction due to laminar boundary layers and quadratic skin friction due to turbulent boundary layers, D_W for wave drift damping, and D_M is for damping due to vortex shedding.

The dynamic equation (3.20) of the NPS ARIES AUV can be expressed by equations (3.24) - (3.29) shown below (Anthony J. Healey, 1993; M. Gertler, 1967). The hydrodynamic coefficient for the equations below uses the value decided through the analysis method of SDV simulator (Richard J. Boncal, 1987; N.S. Smith, 1978).

Surge motion equation

$$\begin{aligned}
 & m[\dot{u} - vr + wq - x_g(q^2 + r^2) + y_g(pq - \dot{r}) + z_g(pr + \dot{q})] \\
 & = \frac{\rho}{2}L^4[X_{pp}p^2 + X_{qq}q^2 + X_{rr}r^2 + X_{pr}pr] \\
 & \quad + \frac{\rho}{2}L^3[X_u\dot{u} + X_wq + X_vp + X_{vr}vr + uq(X_{\phi\delta_s}\delta_s + X_{\phi\delta_b/2}\delta_{bs}) + X_{r\delta_r}ur\delta_r] \\
 & \quad + \frac{\rho}{2}L^2[X_{vv}v^2 + X_{ww}w^2 + X_{v\delta_r}uv\delta_r \\
 & \quad \quad + uw(X_{w\delta_s}\delta_s + X_{w\delta_b/2}\delta_{bs} + X_{w\delta_b/2}\delta_{bp}) \\
 & \quad \quad + u^2(X_{\delta_s\delta_s}\delta_s^2 + X_{\delta_b\delta_b/2}\delta_b^2 + X_{\delta_r\delta_r}\delta_r^2)] \\
 & \quad - (W - B)\sin\theta \\
 & \quad + \frac{\rho}{2}L^3X_{\phi sn}uq
 \end{aligned} \tag{3.24}$$

Sway motion equation

$$\begin{aligned}
 & m[\dot{v} + ur - wp + x_g(pq + \dot{r}) - y_g(p^2 + r^2) + z_g(qr - \dot{p})] \\
 & = \frac{\rho}{2}L^4[Y_p\dot{p} + Y_r\dot{r} + Y_{pq}pq + Y_{qr}qr] \\
 & \quad + \frac{\rho}{2}L^3[Y_v\dot{v} + Y_pup + Y_rur + Y_{vq}vq + Y_{wp}wp + Y_{wr}wr] \\
 & \quad + \frac{\rho}{2}L^2[Y_vuv + Y_{vw}vw + Y_{\delta_r}u^2\delta_r] \\
 & \quad - \frac{\rho}{2}\int_{x_{tail}}^{x_{nose}} [C_{dy}h(x)(v + xr)^2 + C_{dz}b(x)(w - xq)^2] \cdot \frac{(v + xr)}{U_{cf}(x)} dx \\
 & \quad + (W - B)\cos\theta \sin\phi
 \end{aligned} \tag{3.25}$$

Heave motion equation

$$\begin{aligned}
 & m[\dot{w} - uq + vp + x_g(pr - \dot{q}) + y_g(qr + \dot{p}) - z_g(p^2 + q^2)] \\
 &= \frac{\rho}{2} L^4 [Z_q \dot{q} + Z_{pp} p^2 + Z_{pr} pr + Z_{rr} r^2] \\
 &+ \frac{\rho}{2} L^3 [Z_w \dot{w} + Z_q uq + Z_{vp} vp + Z_{vr} vr] \\
 &+ \frac{\rho}{2} L^2 [Z_w ww + Z_{vv} v^2 + u^2 (Z_{\delta s} \delta_s + Z_{\delta b/2} \delta_{bs} + Z_{\delta b/2} \delta_{bp})] \\
 &- \frac{\rho}{2} \int_{x_{tail}}^{x_{nose}} [C_{dy} h(x)(v + xr)^2 + C_{dz} b(x)(w - xq)^2] \cdot \frac{(w - xq)}{U_{cf}(x)} dx \\
 &+ (W - B) \cos \theta \cos \phi \\
 &+ \frac{\rho}{2} L^3 Z_{qn} uq \epsilon(n) + \frac{\rho}{2} L^2 [Z_{wn} ww + Z_{\delta sn} u^2 \delta_s] \epsilon(n)
 \end{aligned} \tag{3.26}$$

Roll motion equation

$$\begin{aligned}
 & I_x \dot{p} + (I_x - I_y)qr + I_{xy}(pr - \dot{q}) - I_{yz}(q^2 - r^2) - I_{xz}(pq + \dot{r}) \\
 &+ m[y_g(\dot{w} - uq + vp) - z_g(\dot{v} + ur - wp)] \\
 &= \frac{\rho}{2} L^5 [K_p \dot{p} + K_r \dot{r} + K_{pq} pq + K_{qr} qr] \\
 &+ \frac{\rho}{2} L^4 [K_v \dot{v} + K_p up + K_r ur + K_{vq} vq + K_{wp} wp + K_{wr} wr] \\
 &+ \frac{\rho}{2} L^3 [K_v uv + K_{vw} vw + u^2 (K_{\delta b/2} \delta_{bp} + K_{\delta b/2} \delta_{bs})] \\
 &+ (y_g W - y_b B) \cos \theta \cos \phi - (z_g W - z_b B) \cos \theta \sin \phi \\
 &+ \frac{\rho}{2} L^4 K_{pn} up \epsilon(n) + \frac{\rho}{2} L^3 K_{pr} pr u^2
 \end{aligned} \tag{3.27}$$

Pitch motion equation

$$\begin{aligned}
 & I_y \dot{q} + (I_x - I_z)pr - I_{xy}(qr + \dot{p}) + I_{yz}(pq - \dot{r}) + I_{xz}(p^2 - r^2) \\
 & \quad - m[x_g(\dot{w} - uq + vp) - z_g(\dot{u} - vr + wq)] \\
 & = \frac{\rho}{2} L^5 [M_{\dot{q}} \dot{q} + M_{pp} p^2 + M_{pr} pr + M_{rr} r^2] \\
 & \quad + \frac{\rho}{2} L^4 [M_{\dot{w}} \dot{w} + M_{uq} uq + M_{vp} vp + M_{vr} vr] \\
 & \quad + \frac{\rho}{2} L^3 [M_{uw} uw + M_{vv} v^2 + u^2 (M_{\delta_s} \delta_s + M_{\delta_b/2} \delta_{bp} + M_{\delta_b/2} \delta_{bs})] \\
 & \quad + \frac{\rho}{2} \int_{x_{mil}}^{x_{nose}} [C_{dy} h(x)(v + xr)^2 + C_{dz} b(x)(w - xq)^2] \cdot \frac{(w - xq)}{U_{cf}(x)} x dx \\
 & \quad - (z_g W - z_b B) \sin \theta \\
 & \quad + \frac{\rho}{2} L^4 M_{qn} uq \epsilon(n) + \frac{\rho}{2} L^3 [M_{un} uw + M_{\delta_{sn}} u^2 \delta_s] \epsilon(n).
 \end{aligned} \tag{3.28}$$

Yaw motion equation

$$\begin{aligned}
 & I_z \dot{r} + (I_y - I_x)pq - I_{xy}(p^2 - q^2) - I_{yz}(pr + \dot{q}) + I_{xz}(qr - \dot{p}) \\
 & \quad + m[x_g(\dot{v} + ur - wp) - y_g(\dot{u} - vr + wq)] \\
 & = \frac{\rho}{2} L^5 [N_{\dot{p}} \dot{p} + N_{\dot{r}} \dot{r} + N_{pq} pq + N_{qr} qr] \\
 & \quad + \frac{\rho}{2} L^4 [N_{\dot{v}} \dot{v} + N_{p} up + N_{r} ur + N_{vq} vq + N_{wp} wp + N_{wr} wr] \\
 & \quad + \frac{\rho}{2} L^3 [N_{uv} uv + N_{vw} vw + N_{\delta_r} u^2 \delta_r] \\
 & \quad - \frac{\rho}{2} \int_{x_{mil}}^{x_{nose}} [C_{dy} h(x)(v + xr)^2 + C_{dz} b(x)(w - xq)^2] \cdot \frac{(v + xr)}{U_{cf}(x)} x dx \\
 & \quad + (x_g W - x_b B) \cos \theta \sin \phi + (y_g W - y_b B) \sin \theta \\
 & \quad + \frac{\rho}{2} L^3 N_{pr} u^2
 \end{aligned} \tag{3.29}$$

x of an integral term is the value for X axis in the body-fixed coordinate system representing the length of AUV model. Although the integral terms of the dynamic equations should be continuously integrated depending on the length of the nose to the tail to calculate for force and moment caused by the fluid, the integral terms in the simulation program of this study are calculated by a Gauss quadrature, assigning 4 points for the AUV model's overall length. Also, the NPS ARIES AUV model is established with a pair of steering rudders and fins for both nose and tail, and a propeller with the intention of control. Control input for each element is as shown in equation (3.30).

$$\delta = [\delta_r \quad \delta_{bs} \quad \delta_{bp} \quad \delta_s \quad \delta_n \quad \delta_B] \quad (3.30)$$

where δ_r is for the steering rudder's angle of the tail, δ_{bs} for the fin's angle of the nose starboard, δ_{bp} for the fin's angle of the nose port, δ_s for the fin's angle of the tail, δ_n for the rev count of the propeller and δ_B is for the adjustment of buoyancy. The simulation program of this study will control δ_r , δ_s and δ_n in order to control the velocity, heading angle and depth of AUV model.

The equation (3.20) can be fixed with equation (3.31) in order to calculate the AUV model's linear and angular velocities variation $\dot{\nu}$ in the body-fixed coordinate system.

$$\dot{\nu} = M^{-1} \cdot [-C(\nu)\nu - D(\nu)\nu - g(\eta) + \tau] \quad (3.31)$$

where the inertia matrix M is shown in equation (3.32).

The ocean comes in complex and irregular forms of current due to various factors including the temperature difference of fluids, tide generating forces owing to the moon and the sun, wind and the surrounding geographic features. Hence, it is difficult to model it mathematically and to consider the influence of the factors on the AUV. Also, considering the influence of the current affecting the motion of AUV, the current will be applied directly to the velocity of the AUV in the NED coordinate system, because it is highly complex to calculate the current force and moment working on the AUV and apply it to the dynamic equation. 2-dimensional current models will be considered instead of complex 3-dimensional models because the navigation algorithm in this study is used to estimate the position of AUV in 2-dimensional XY plane.

The current model applied in the simulation of this study is initially given with the fluid velocity V_c and the flowing direction ψ_c in the NED coordinate system, and can be expressed as equation (3.33).

$$\mathbf{v}_c^n = \begin{bmatrix} u_c \\ v_c \\ w_c \end{bmatrix} = \begin{bmatrix} V_c \cos \psi_c \\ V_c \sin \psi_c \\ 0 \end{bmatrix} \quad (3.33)$$

By applying the current model expressed in the NED coordinate system directly to the coordinate transformation matrix of the equation (3.1) as shown in equation (3.34), the AUV model of the simulation program will move considering the current model, assuming there is no rotational motion of the current.

$$\begin{bmatrix} \dot{\mathbf{p}}_{b/n}^n \\ \dot{\boldsymbol{\theta}}_{nb} \end{bmatrix} = \begin{bmatrix} \mathbf{R}_b^n(\boldsymbol{\theta}_{nb}) & \mathbf{0}_{3 \times 3} \\ \mathbf{0}_{3 \times 3} & \mathbf{T}_{\boldsymbol{\theta}}(\boldsymbol{\theta}_{nb}) \end{bmatrix} \begin{bmatrix} \mathbf{v}_{b/n}^b \\ \boldsymbol{\omega}_{b/n}^b \end{bmatrix} + \begin{bmatrix} \mathbf{v}_c^n \\ \mathbf{0} \end{bmatrix} \quad (3.34)$$

3.3 Sensor model

By considering the characteristics of the sensors used in the actual AUV as shown in **Table 3.2**, the simulation program will generate the measurements of the sensor for the movement of the AUV model. The noise characteristics of each sensor will be decided by referring to the specifications found on the data sheet of sensors or through extra sensor tests. The frequency of data delivery will be decided considering the output frequency of the sensors. The variables X_{GPS} and Y_{GPS} for the GPS measurements are not the values expressed as longitude and latitude in the Earth-Centered Earth-Fixed (ECEF) coordinate system but the values expressed as meter units in the Transverse Mercator (TM) coordinate system. Also, considering that GPS is unable to receive the positional data for the NED coordinate system when submerged, the GPS positional data will not be updated when the depth is deeper than the depth of 0.3m.

Table 3.2 Sensor model specifications

Sensor	Variables	Accuracy	Frequency
GPS	X_{GPS} Y_{GPS}	$\pm 0.3\text{m}$	10 Hz
Pressure	Z_{Press}	0.043 %FS	10 Hz
Magnetic compass	ψ_{Mag}	$\pm 0.5^\circ$	10 Hz
DVL	u_{DVL} v_{DVL}	1% $\pm 1\text{mm/s}$	2 Hz
Gyro	r_{Gyro}	$\pm 0.05^\circ/\text{s}/\sqrt{\text{Hz}}$	10 Hz

3.4 Controller

PD or PID controllers for speed, heading angle and depth will be established in order to carry out way-points control simulation of the AUV model. Each controller will be given the rotation speed of the propeller δ_n , the angle of steering rudder δ_r and the angle of fin δ_s . The maximum angle for the steering rudder and fin will be limited to $\pm 35^\circ$.

Speed controller

Equation (3.35) is PID controller for speed and its output value is the rotation speed of the propeller δ_n .

$$\delta_n = K_{sp}e_u + K_{si} \int e_u dt + K_{sd}\dot{e}_u \quad (3.35)$$

where K_{sp} , K_{si} and K_{sd} respectively represent the proportional gain, integral gain and differential gain of PID controller for speed, and e_u represents the difference between desired surge velocity u_{des} and the surge velocity of the AUV model.

Heading controller

Equation (3.36) is PD controller for heading angle and its output value is the rotated angle δ_r of the steering rudder.

$$\delta_r = -[K_{hp}e_\psi + K_{hd}\dot{e}_\psi] \quad (3.36)$$

where K_{hp} and K_{hd} respectively represent the proportional gain and differential gain of PD controller of the heading angle, and e_ψ represents the difference between the desired heading angle ψ_{des} and the AUV model's heading angle.

Depth & pitch controller

It is general to consider the depth together with the pitch to the Y_o axis in a body-fixed coordinate system for the performance of the controller and stable operation of the AUV. Equation (3.37) is PD controller for depth and its output value is the rotated angle δ_s of the fin.

$$\delta_s = K_{dp}e_Z + K_{dd}\dot{e}_Z - [K_{pp}e_\theta + K_{pd}\dot{e}_\theta] \quad (3.37)$$

where K_{dp} and K_{dd} respectively represent the proportional gain and differential gain of PD controller for depth, while K_{pp} and K_{pd} represent the proportional gain and differential gain of rotation based on Y_o axis respectively. Also, e_Z represents the difference of the desired depth Z_{des} and the depth where AUV model is located.

3.5 Scenarios

In order to verify the performance of the GPS-aided navigation algorithm suggested on this study, the simulation will conduct 3 scenarios depending on the kind of simulation and the applicability of navigation algorithms. Each scenario is established as shown in **Table 3.3**.

Table 3.3 Scenarios list

No	Simulation type	Estimation usage	Estimation time	Surge Velocity u	Current (V_c / ψ_c)
1	Way-point	False	-	3 kn	-
2	Way-point	True	Initial	3 kn	0.5 kn / 60°
3	Straight	True	Always	3 kn	-

First, arbitrary bias error b_{ψ}^{ref} for geodetic north included in the heading angle ψ_{Mag} measured by the magnetic compass in scenario 1 and 2, and the initial position, attitude and velocity of the AUV during a way-point control simulation will be configured equally. The configured values are as shown in equation (3.38) and (3.39).

$$b_{\psi}^{ref} = -15^{\circ} \quad (3.38)$$

$$[X_0 \ Y_0 \ Z_0 \ \phi_0 \ \theta_0 \ \psi_0 \ u_0 \ v_0 \ w_0] = [0 \ 0 \ 2 \ 0 \ 0 \ 0 \ 1 \ 0 \ 0] \quad (3.39)$$

When the AUV is moving straight to the geodetic north in the NED coordinate system, heading bias error of -15° let dead reckoning using magnetic compass leave movement traces towards geodetic north 15° . The AUV model will be initially configured with the heading angle of 0° , surge velocity of 1kn, and a depth of 2m.

The way-points designated in the way-point control simulation for scenarios 1 and 2 are located in the NED coordinate system as shown in equation (3.40).

$$\begin{array}{ll}
 \text{WP (1)} : & (0, 0, Z_{WP}(1)) \\
 \text{WP (2)} : & (200, 0, Z_{WP}(2)) \\
 \text{WP (3)} : & (200, 300, Z_{WP}(3)) \\
 \text{WP (4)} : & (150, 300, Z_{WP}(4)) \\
 \text{WP (5)} : & (150, 100, Z_{WP}(5)) \\
 \text{WP (6)} : & (100, 100, Z_{WP}(6)) \\
 \text{WP (7)} : & (100, 300, Z_{WP}(7)) \\
 \text{WP (8)} : & (-50, 300, Z_{WP}(8)) \\
 \text{WP (9)} : & (-50, 100, Z_{WP}(9)) \\
 \text{WP (10)} : & (-100, 100, Z_{WP}(10))
 \end{array} \quad (3.40)$$

The coordinates of way-points for XY plane in the NED coordinate system are applied equally for the two scenarios and their depth Z_{WP} will be differently configured depending on the use of the proposed navigation algorithm. For scenario 1, it will move under water without using the navigation algorithm as shown in equation (3.41) and for scenario 2, it will move on the water at the early part of the simulation and then under water as shown in equation (3.42).

$$Z_{WP}^1 = [2 \ 2 \ 2 \ 2 \ 2 \ 2 \ 2 \ 2 \ 2 \ 2] \quad (3.41)$$

$$Z_{WP}^2 = [2 \ 0 \ 2 \ 2 \ 2 \ 2 \ 2 \ 2 \ 2 \ 2] \quad (3.42)$$

In scenario 1 which uses way-points for depth Z_{WP}^1 , the AUV will move with the depth of 2m during the entire simulation and will move relying on dead reckoning without receiving GPS positional data. In scenario 2 which uses Z_{WP}^2 , the AUV model's position and heading bias error of the magnetic compass to geodetic north will be estimated by receiving GPS positional data. For underwater movement, dead reckoning will be used considering the position and heading bias error, which are estimated during the last movement on the water.

Scenario 3 will perform a heading control simulation moving straight with the heading angle of 0° . By continuously conducting navigation algorithm through movement on the water, the navigation algorithm estimates the magnetic compass' heading bias error b_ψ^{ref} , which is arbitrarily configured as shown in equation (3.43), and the AUV model's position. The initial position, attitude and velocity of the AUV will be initially configured as shown in equation (3.44).

$$b_\psi^{ref} = -5^\circ \quad (3.43)$$

$$[X_0 \ Y_0 \ Z_0 \ \phi_0 \ \theta_0 \ \psi_0 \ u_0 \ v_0 \ w_0] = [0 \ 0 \ 0 \ 0 \ 0 \ 0 \ 1 \ 0 \ 0] \quad (3.44)$$

where a heading bias error b_ψ^{ref} of the magnetic compass will be configured as -5° , which is similar with the heading bias error estimated in the field test. The simulation results of scenario 3 will be compared with the result of the field test. The AUV model in the simulation will be initially configured with the depth of 0m, heading angle of 0° and surge velocity of 1kn for start.

The AUV model in every simulation scenario will have the surge velocity of 3kn. For scenario 2 which considers the effect of current, the velocity V_c of the current will be configured as 0.5kn and the heading angle ψ_c of the current

will be configured as 60° in geodetic north.

3.6 Simulation results

This section shows the graphic results of the dynamic simulations by scenarios mentioned in **Table 3.3**, and compares the movement traces of the AUV depending on the reception of GPS positional data. The reception of GPS positional data reflects whether the navigation algorithm, which estimates the heading bias error of the magnetic compass and the position of the AUV model, was conducted or not. The simulation graphic results afterwards are classified with different colors as shown in **Table 3.4**.

Table 3.4 Colored graphs classification

Color	Description
Black	Referenced (or criterion)
Blue	Measured by sensor
Green	Estimated by proposed navigation algorithm
Red	Desired

Scenario 1

Dead reckoning by a magnetic compass and a DVL was used for movement without GPS positional data by designating the 10 way-points including the initial position as way-points underwater. The simulation was conducted without

the current. The movement traces of the AUV model in the NED coordinate system is as shown in Fig. 3.5.

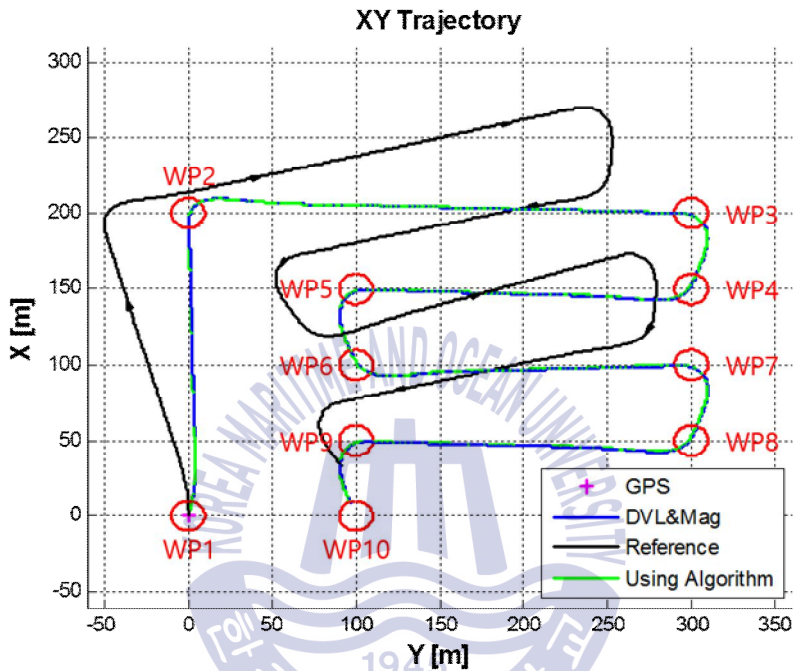


Fig. 3.5 Scenario 1, XY trajectory

Red circles represent the effective radius of 10 way-points, which exist on the center of each circle. The position of the AUV model was estimated by using dead reckoning without considering the magnetic compass' heading bias error. The movement traces are shown in blue lines, while the black lines represent the movement traces the AUV model actually moved. The green lines are movement traces of the AUV model estimated by navigation algorithm. Since GPS positional data was not received in scenario 1, they show similar movement traces as the blue lines.

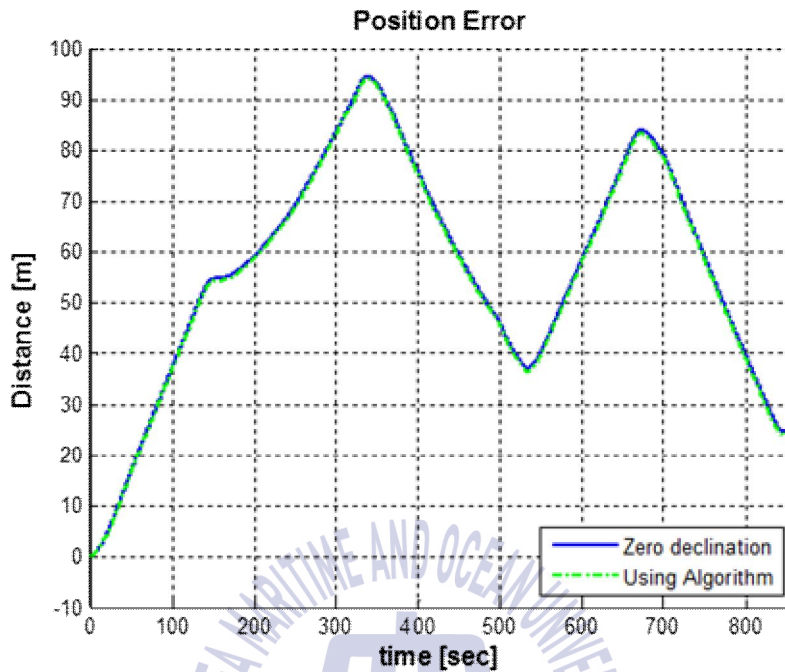


Fig. 3.6 Scenario 1, Position error

Dead reckoning without considering the heading bias error of a magnetic compass, using a heading bias error of 0° , shows a difference with the actual position of the AUV model as expressed in the NED coordinate system shown in the blue lines in **Fig. 3.6**. The green dotted lines represent the position error of the AUV model, estimated with the navigation algorithm. It shows similar position errors using dead reckoning since the heading bias error was not estimated.

When the AUV model is running, the position error caused by the discordance of the reference coordinate system for navigation largely occurs depending on the planned course.

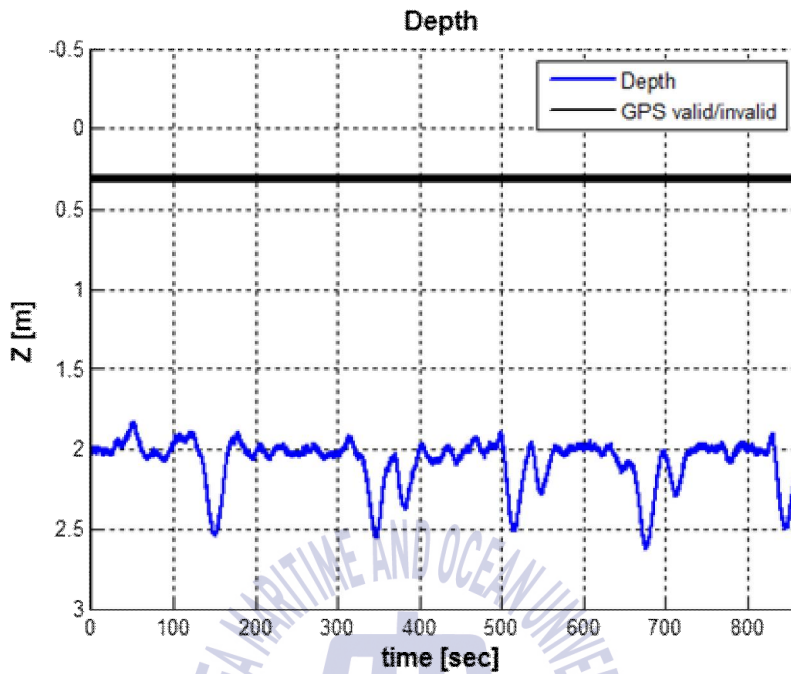


Fig. 3.7 Scenario 1, Depth

In **Fig. 3.7**, black lines show the depth of 0.3m which determine the validity of GPS, and depth below the line is not valid for GPS. Blue lines show the depth of the AUV model controlled with a depth of 2m. We can see that changes occur in the depth when the AUV model performs rotational motions at each way-point.

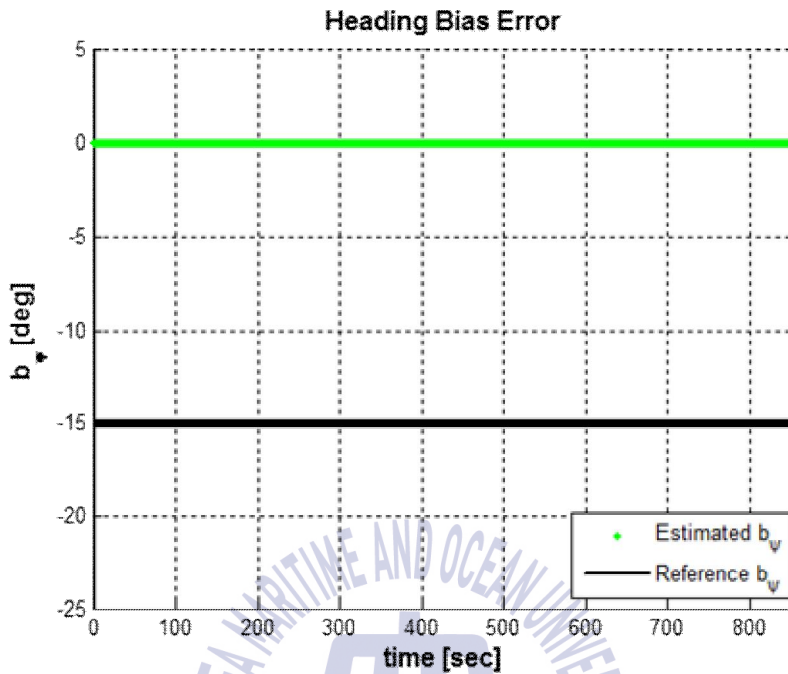


Fig. 3.8 Scenario 1, Heading bias error

Scenario 1 simulation is not able to receive the GPS positional data and does not estimate the heading bias error of the magnetic compass due to the continuous underwater movement of the AUV model during the entire simulation. Therefore, we can identify that the estimated heading bias error of the navigation algorithm expressed as a green dotted line in **Fig. 3.8** does not estimate the heading bias error of the black line configured in the equation (3.38). Since the navigation algorithm maintains the final estimated value when the GPS data is not valid, scenario 1 conducts dead reckoning by considering the heading bias error with the initially configured value of 0° .

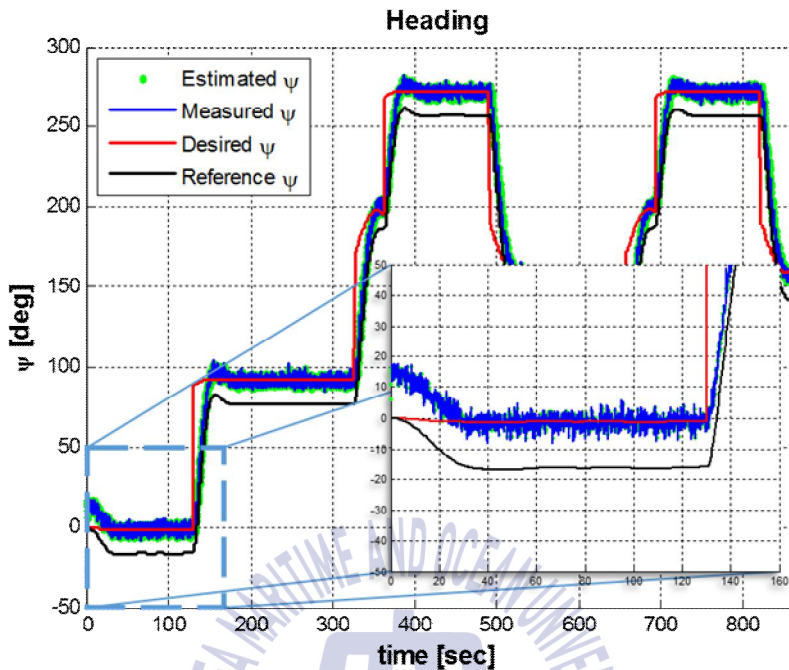


Fig. 3.9 Scenario 1, Heading angle

The heading angle of the AUV model is expressed in **Fig. 3.9**. By applying the LOS method, desired heading angle for the next way-point in the current position will be obtained as shown in the red line and the steering rudder angle δ_r will be controlled to follow it. The significance for each graph is shown in the legend. Due to the heading bias error configured in the equation (3.38), the measurements of the sensor for the heading angle and the estimated heading angle of the navigation algorithm are controlled to be similar with the desired heading angle. The black line indicates the actual heading angle of the AUV model.

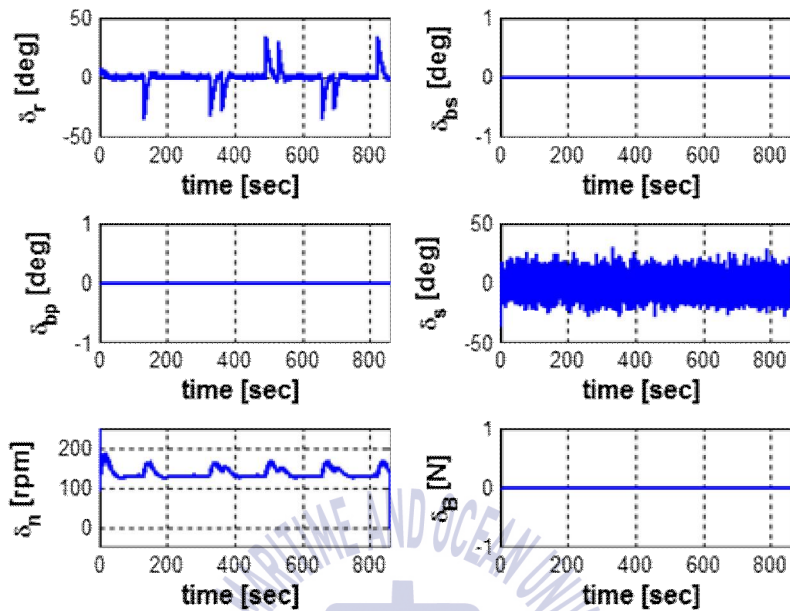


Fig. 3.10 Scenario 1, Control inputs

The control of the thruster rev count δ_n , the steering rudder angle δ_r and the fin angle δ_s is shown in **Fig. 3.10** for a way-point control simulation. The surge velocity following the desired velocity 3kn is shown in the green line of **Fig. 3.11**. It can be confirmed that the velocity changes every time when the AUV model travels each way-point.

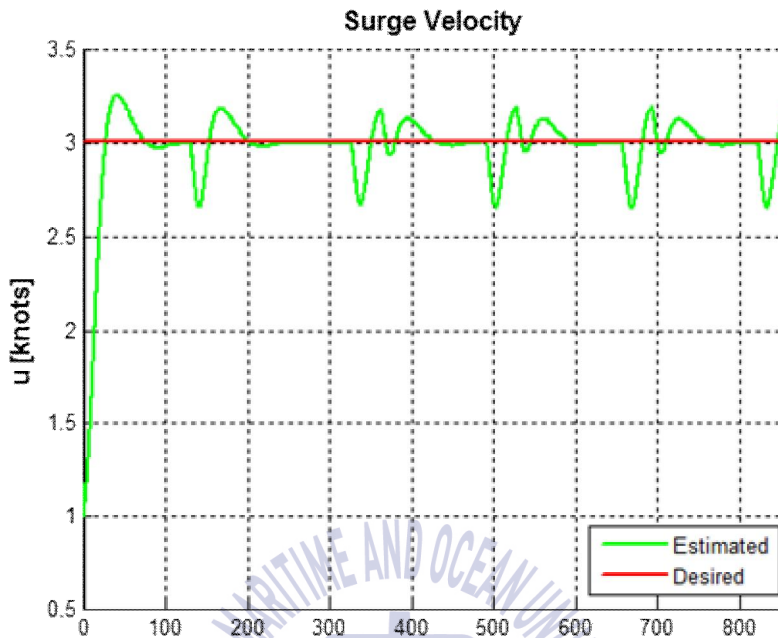


Fig. 3.11 Scenario 1, Surge velocity

Scenario 2

Although the position of the way-points on the XY plane in scenario 2 is the same with scenario 1, the navigation algorithm in scenario 2 estimates the position of the AUV model and the heading bias error of the magnetic compass based on geodetic north, since the AUV model receives the GPS positional data expressed in magenta '+' when moving on the water from WP1 to WP2. Considering estimated values, the way-point control simulation will be conducted by dead reckoning when moving underwater. The current model that is considered as separate disturbance has the velocity of 0.5kn and flowing direction of 60° based on geodetic north. The XY trajectory of the AUV model in the NED coordinate system is shown in **Fig. 3.12**.

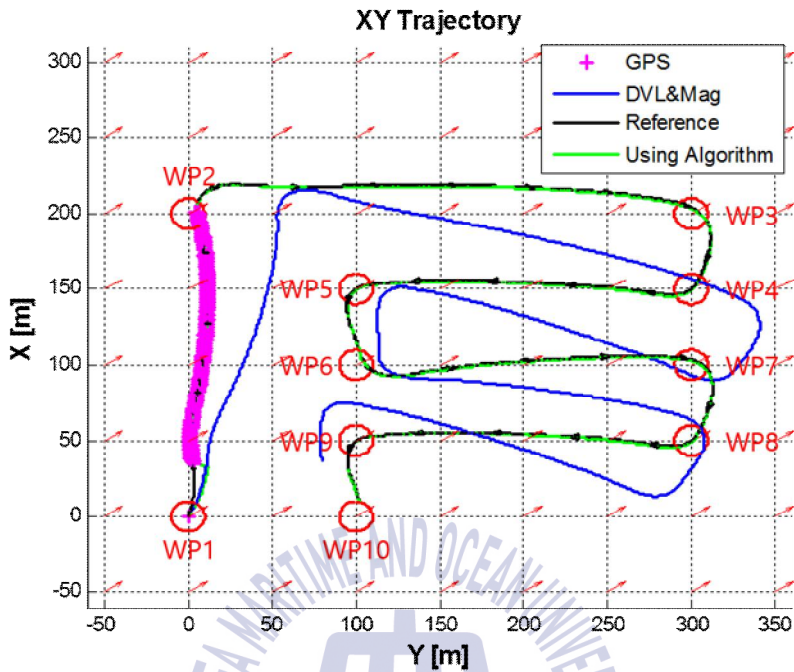


Fig. 3.12 Scenario 2, XY trajectory

Similarly with scenario 1, the way-point control simulation, which travels 10 points, will be conducted. Each way-point will be located on the center of the effective radius shown in red circles. The actual trajectory of the AUV based on the NED coordinate system is shown in the black line, and the position of the AUV model estimated by dead reckoning which did not consider the heading bias error is shown in the blue line. The trajectory of the AUV model with the navigation algorithm considering the heading bias error is estimated in the green line. The navigation algorithm considers the magnetic compass' heading bias error from the movement on the water. It can be seen that the estimated position is similar with the actual position of the AUV model when submerged. Meanwhile, we can see that the trajectory of the AUV model estimated without considering the heading bias error shows a great difference with the actual position of the AUV model in the NED coordinate system.

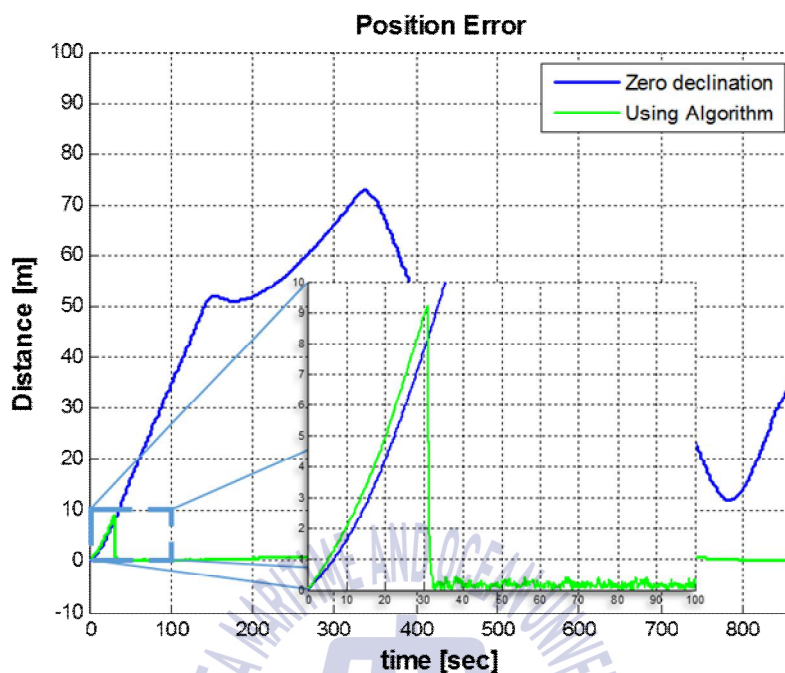


Fig. 3.13 Scenario 2, Position error

Fig. 3.13 shows the differences of two positions estimated by dead reckoning and the navigation algorithm with the actual position of the AUV model in blue and green line respectively. The position error is shown to be accumulated more as time goes by before floating on the water since the AUV model starts from the depth of 2m in scenario 2. However, we can see that the position error is greatly improved when the AUV model receives the GPS positional data and fixes the position error after 32.1 seconds. The depth of the AUV model is shown in the depth measurements expressed in the blue line of **Fig. 3.14**.

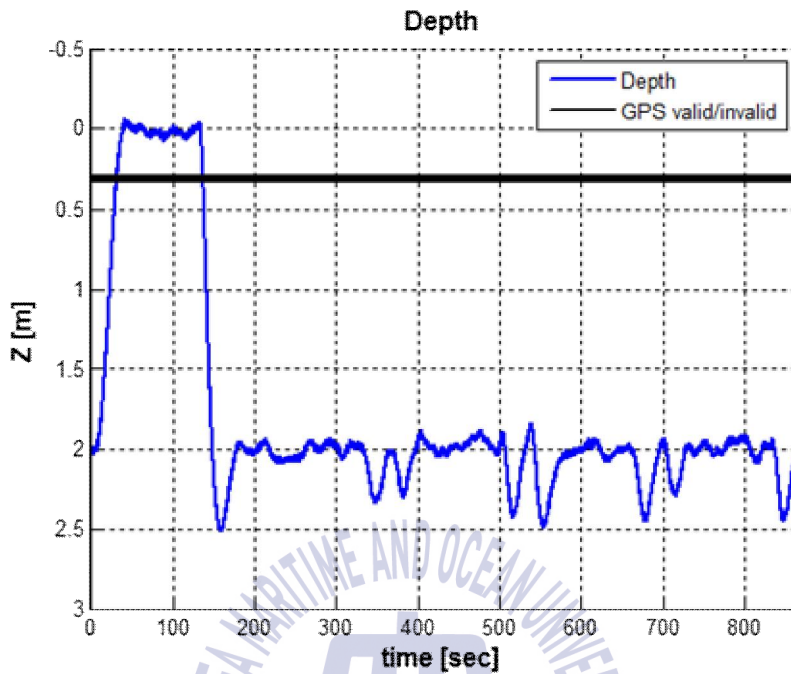


Fig. 3.14 Scenario 2, Depth

The black line shows the depth of 0.3m. When the depth gets lower than this, during the time between 32.1~137.5 seconds, the GPS positional data is received. The AUV model moves initially from the depth of 2m and floats on the water, afterwards it estimates the position and heading bias error of the AUV model by receiving the GPS positional data.

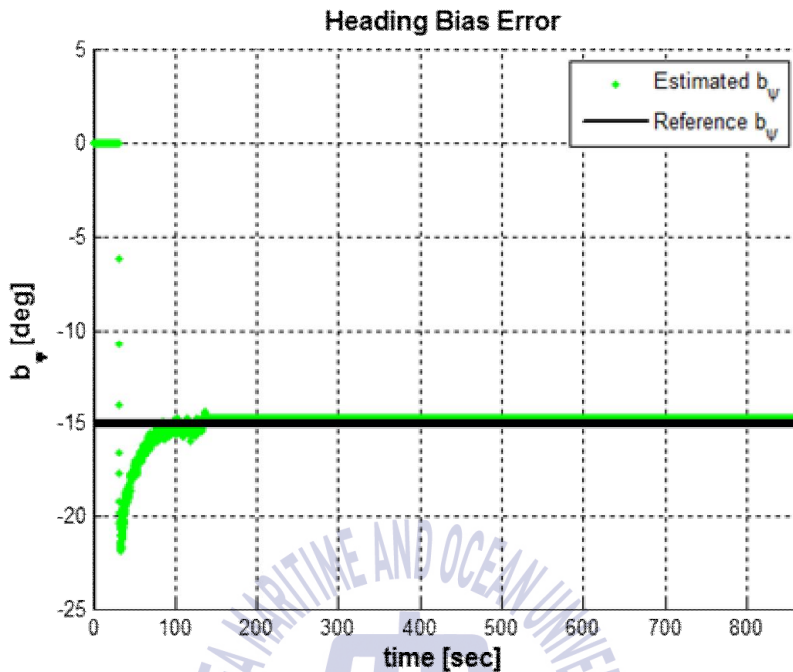


Fig. 3.15 Scenario 2, Heading bias error

The navigation algorithm estimates the heading bias error b_ψ of the magnetic compass based on geodetic north during the simulation, which is expressed in the green line shown in **Fig. 3.15**.

We can see that the estimated heading bias error of the navigation algorithm is gradually following the heading bias error configured in the equation (3.38) since it receives the GPS positional data when the AUV surfaced. The heading bias error is estimated by receiving the GPS positional data during the time between 32.1~137.5 seconds. When moving underwater, the simulation is conducted by considering the final estimated value for the heading bias error. The heading bias error of -14.79° is considered in the simulation when submerged. It can be seen that the estimated heading bias error is similar with the arbitrary heading bias error expressed as a black line.

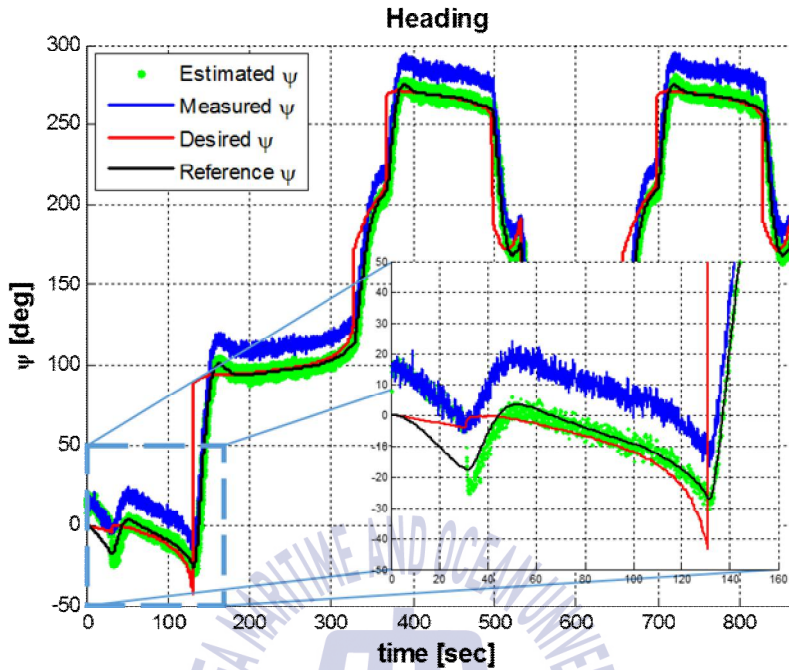


Fig. 3.16 Scenario 2, Heading angle

The heading angle of the AUV model in scenario 2 is shown in **Fig. 3.16**. The desired heading angle for next way-point will be obtained as shown in the red line in the current position. The steering rudder angle δ_r will be controlled to follow it. The significance for each graph will be shown in the legend.

Due to the heading bias error of the AUV model shown as a black line in **Fig. 3.15**, the sensor measurements for the heading angle of the AUV model shown as a blue line in **Fig. 3.16** shows a considerable difference between the actual AUV model's heading angle shown as a black line in **Fig. 3.16** in all sections. By considering the heading bias error estimated in the section of 32.1~137.5 seconds, we can see that the estimated heading angle of the navigation algorithm shown as a green line is similar with the actual heading angle of the AUV model based on the NED coordinate system.

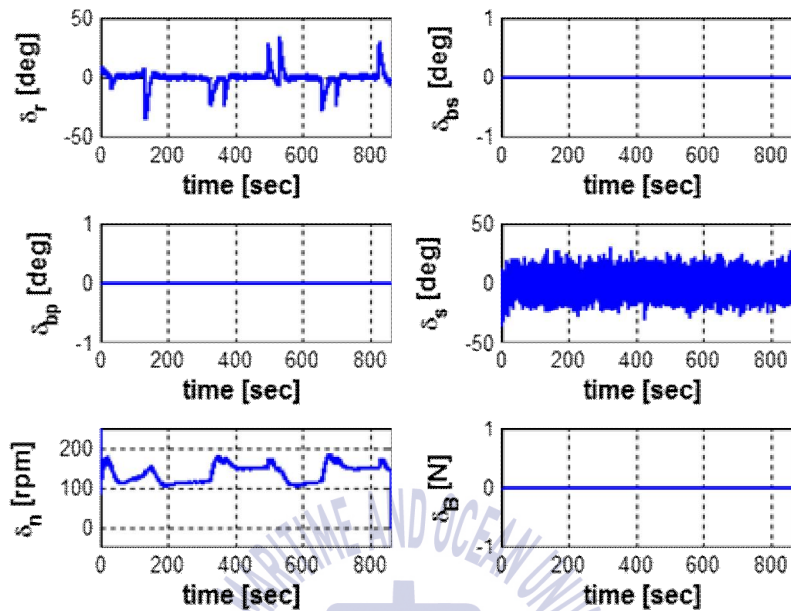


Fig. 3.17 Scenario 2, Control inputs

The rev count δ_n of the propeller, angle of the steering rudder δ_r , and angle of the fin δ_s are controlled as shown in **Fig. 3.17** for a way-point control simulation. The surge velocity following the desired velocity 3kn can be seen in the green line of **Fig. 3.18**. It can be confirmed that the velocity changes every time the AUV model travels for each way-point.

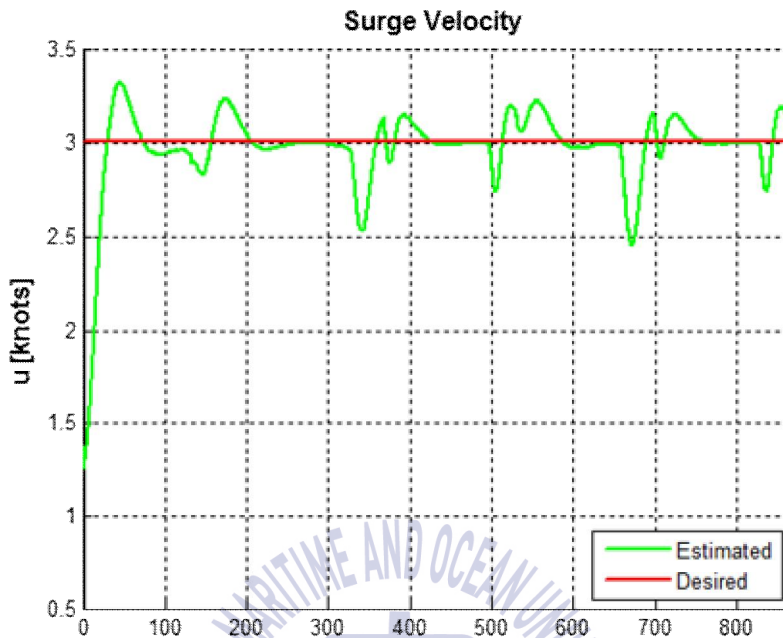


Fig. 3.18 Scenario 2, Surge velocity

Scenario 3

Scenario 3 simulation controls the heading angle moving straight to the desired heading angle of 0° . Through movement on the water, it continuously receives GPS positional data expressed as magenta '+' in **Fig. 3.19**. The navigation algorithm then estimates the position of the AUV model and the heading bias error of the magnetic compass based on geodetic north.

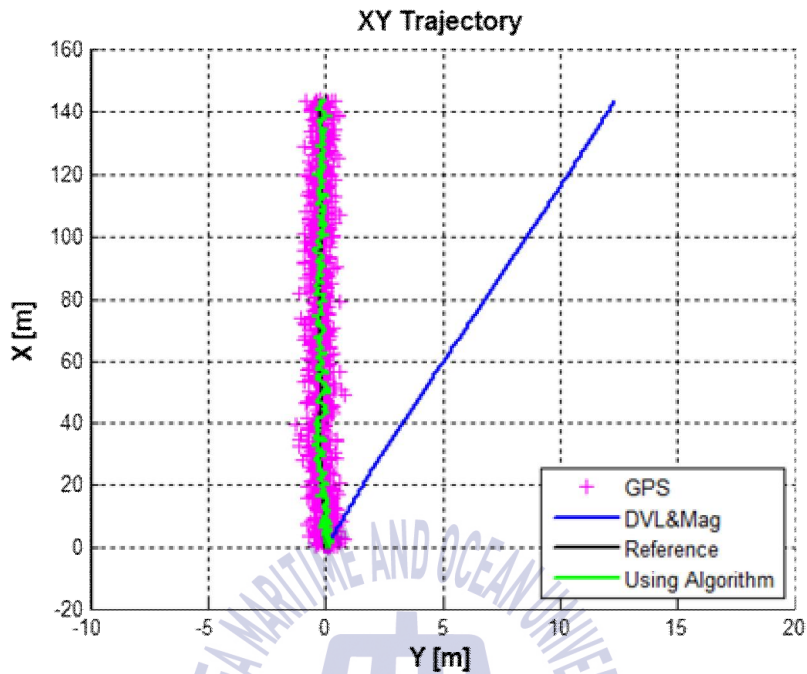


Fig. 3.19 Scenario 3, XY trajectory

When the AUV model actually moves following the black line, dead reckoning using the measurements of a magnetic compass and DVL estimates the position of the AUV model in the blue line, which draws a biased trajectory compared to the actual trajectory of the AUV model. This greatly resulted from the heading bias error b_{ψ}^{ref} , which was arbitrarily configured in the equation (3.43). Each navigation system draws different trajectories due to the different reference coordinate system. Meanwhile, the GPS-aided navigation algorithm estimates the position of the AUV model as shown in green line through the GPS positional data. We can see that it is similar with the actual position of the AUV. When conducting the scenario 3 simulation, the differences between the actual position of the AUV model and the position estimated by each navigation system will be shown in **Fig. 3.20**.

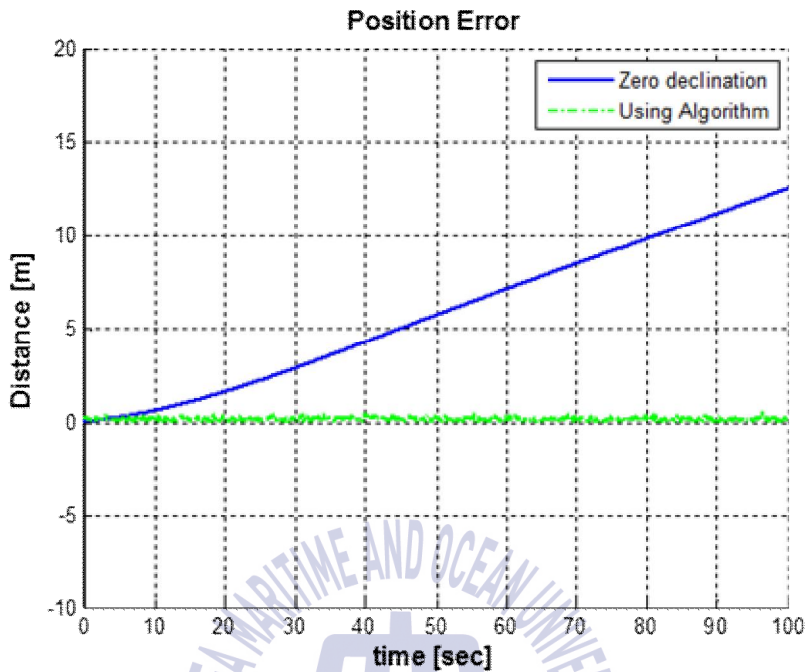


Fig. 3.20 Scenario 3, Position error

When the AUV model's heading angle was decided by the measurements of the magnetic compass, without considering the heading bias error, we can see that the position error is accumulated as expressed in the blue line. Meanwhile, the navigation algorithm using GPS as an auxiliary sensor shows the position error of almost 0m.

The AUV model in the scenario 3 simulation moves straight with the desired depth of 0m. It gradually accelerated to the velocity of 3kn when the simulation starts. Fluid resistance of acceleration and velocity applies to the AUV model and causes it to generate force and moment. The controller in the equation (3.37) was used in order to get over various disturbances and to follow the desired depth. The depth of the AUV model expressed as a blue line in **Fig. 3.21** converges within the range of 0.1m for the desired depth.

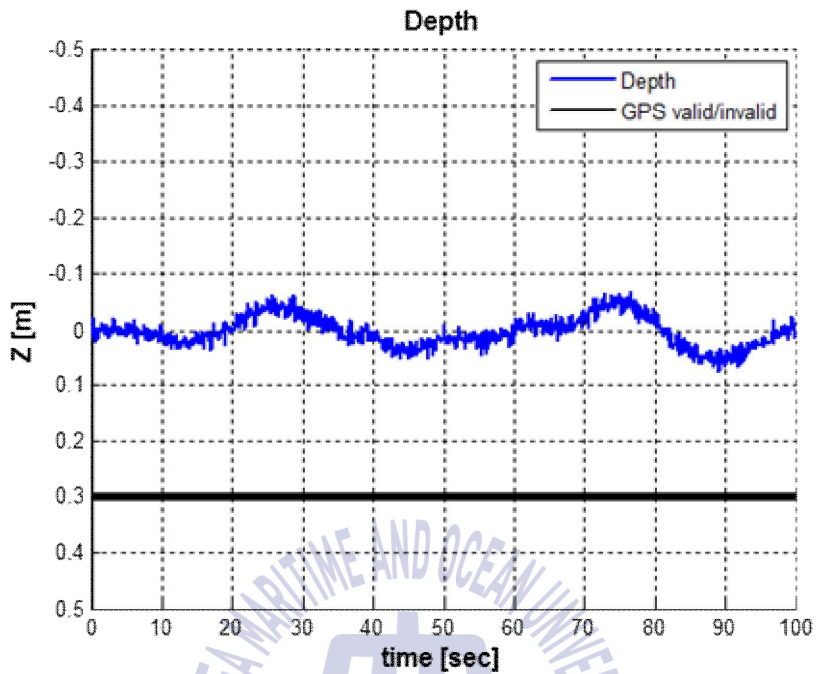


Fig. 3.21 Scenario 3, Depth

The Black line represents the depth of 0.3m. The navigation algorithm receives GPS positional data when the AUV located in a shallower depth than the black line. The AUV model starts from the depth of 0m. The navigation algorithm estimates the AUV model's position and the heading bias error, by receiving GPS positional data through continuous movement on the water.

The estimated heading bias error of the magnetic compass when the AUV model travels on the water in the heading control simulation of scenario 3 is shown as dotted green lines in **Fig. 3.22**.

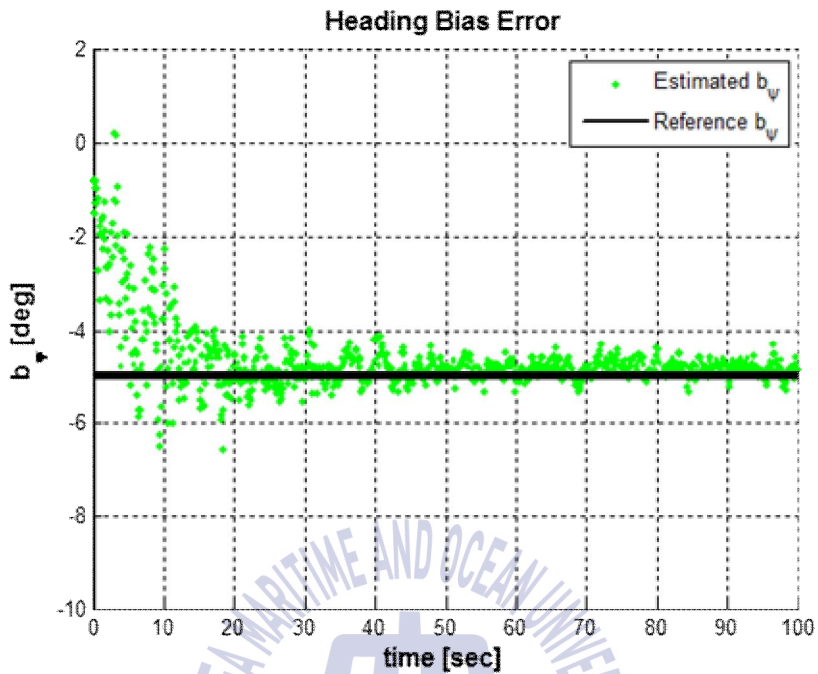


Fig. 3.22 Scenario 3, Heading bias error

The heading bias error of the magnetic compass was set as -5° in the equation (3.43) and expressed as a black line. The estimated heading bias error converges within the range of $\pm 1^\circ$ for the actual heading bias error.

The heading angle of the AUV model in the heading control simulation of scenario 3 is shown in **Fig. 3.23**. The AUV model is controlled by following the desired heading angle 0° , which is expressed as a red line. The significance for each graph is described in the legend.

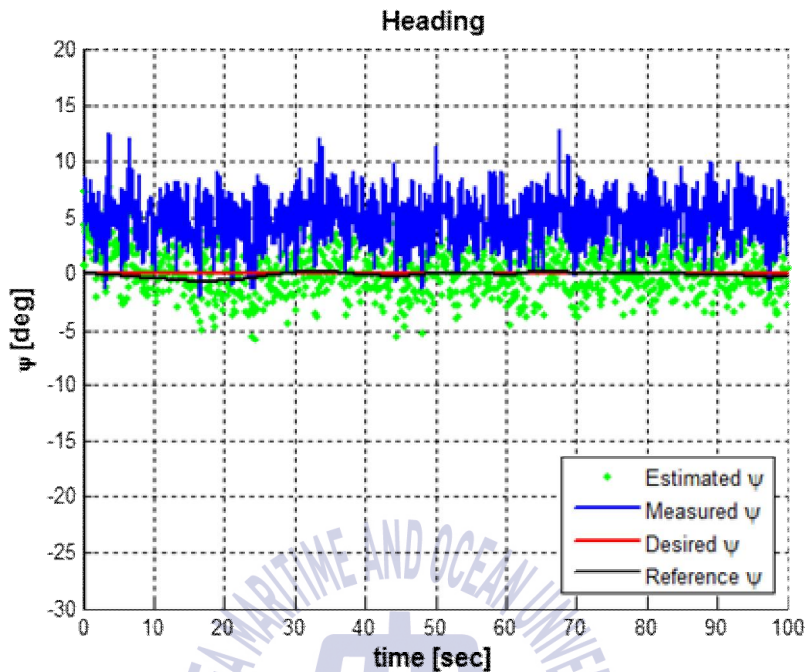


Fig. 3.23 Scenario 3, Heading angle

Due to the initial configured heading bias error of -5° , the blue line, which represents the measurements of the sensor for the heading angle of the AUV model, shows consistent differences with the black line in all sections. The black line represents the actual heading angle to geodetic north.

Considering the heading bias error estimated by the navigation algorithm when surfaced, the estimated heading angle of the navigation algorithm expressed in green line shows a similar value with the actual heading angle of the AUV model in the NED coordinate system, expressed in black line.

The control of the thruster rev count δ_n , the steering rudder angle δ_r and the fin angle δ_s is shown in **Fig. 3.24** for the heading control simulation. The surge velocity of the AUV model following the desired velocity of 3kn can be seen in the green line of **Fig. 3.25**.

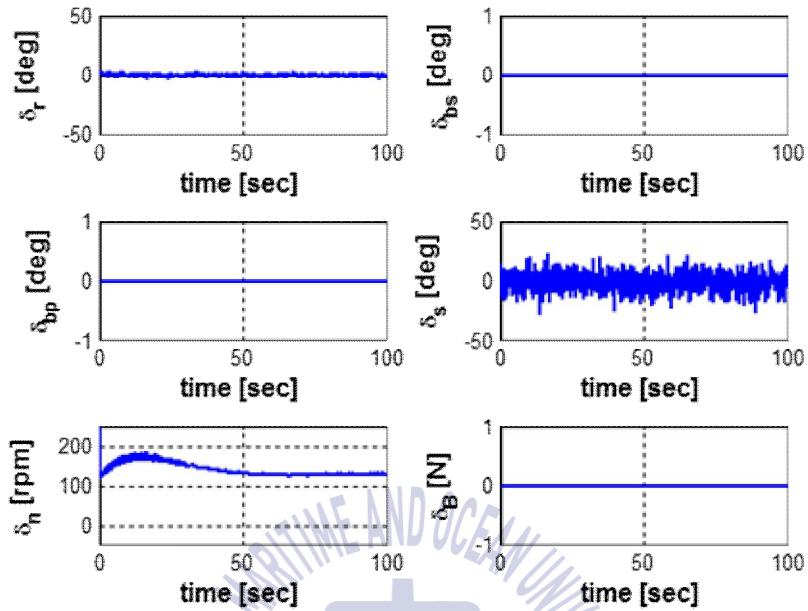


Fig. 3.24 Scenario 3, Control inputs

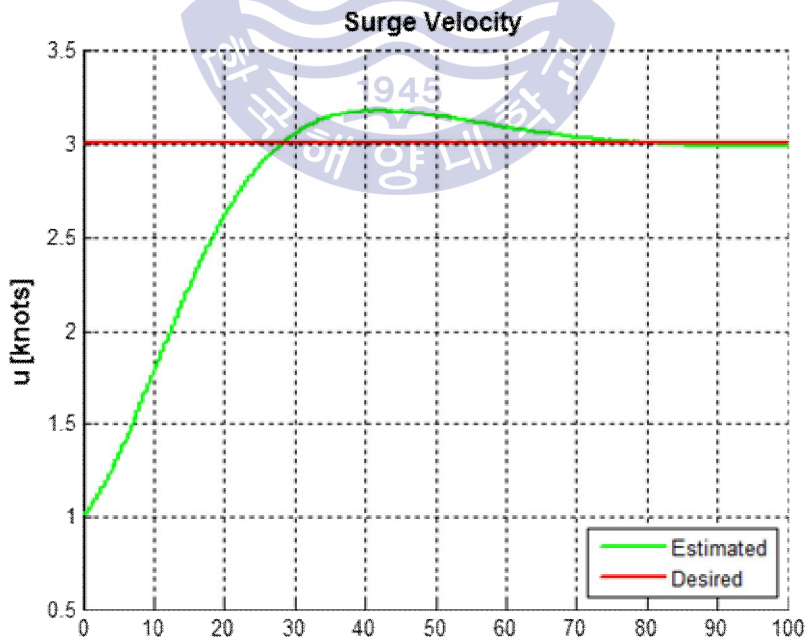


Fig. 3.25 Scenario 3, Surge velocity

CHAPTER 4 FIELD TEST

4.1 Hovering-type AUV platform

KMOU has been conducting studies about UUVs on both theories and field tests. This chapter introduces the hovering-type AUV platform, which is used in several field tests for the analysis of dynamic characteristics, performance verification of control algorithm (Dong-ho Choi, 2016).

4.1.1 Dimensions and specifications

The dimensions and specifications of the hovering-type AUV are shown in **Table 4.1**. The hovering-type AUV is a test-bed for the analysis of the AUV's dynamic characteristics and performance verification of control and navigation algorithm. It was developed in an open-frame form and considered the availability of sensor mounting and field test.

In order to conduct the test with the minimum number of staff, the size and weight of the AUV were determined as follows. The battery capacity was selected by analyzing the energy consumption of the system for it to conduct the test for more than two hours in the ocean. In order to operate the AUV in the ocean, the operating depth of 10m was established. Considering the operating depth, sensors were chosen and a pressure vessel was designed. Two horizontal propellers and two vertical propellers were installed for the 4-DOF movement. GPS, DVL, TCM, AHRS and a pressure sensor were installed in

order to measure the velocity, position and attitude of the AUV. Onboard PC LabVIEW and C++ of Edison board were used to develop the operating and navigation systems of the AUV.

Table 4.1 Hovering-type AUV specifications

Parameter	Specification
Dimension (L×W×H)	736 mm × 736 mm × 600 mm
Weight	50 kgf (in air)
Operating depth	10 m
Battery	25.9 V – 6600 mA LiPo × 6 EA
Sensor	GPS / DVL / TCM / AHRS / Pressure sensor
Thruster	Tecnadyne model 300 × 2 EA Tecnadyne model 280 × 2 EA
Control mode	4-DOF
Control board	On board PC / Intel Edison board / NI USB-6009 / NI cDAQ-9264
Operating program	Windows NI LabVIEW / Linux C++

4.1.2 Boards

On board PC

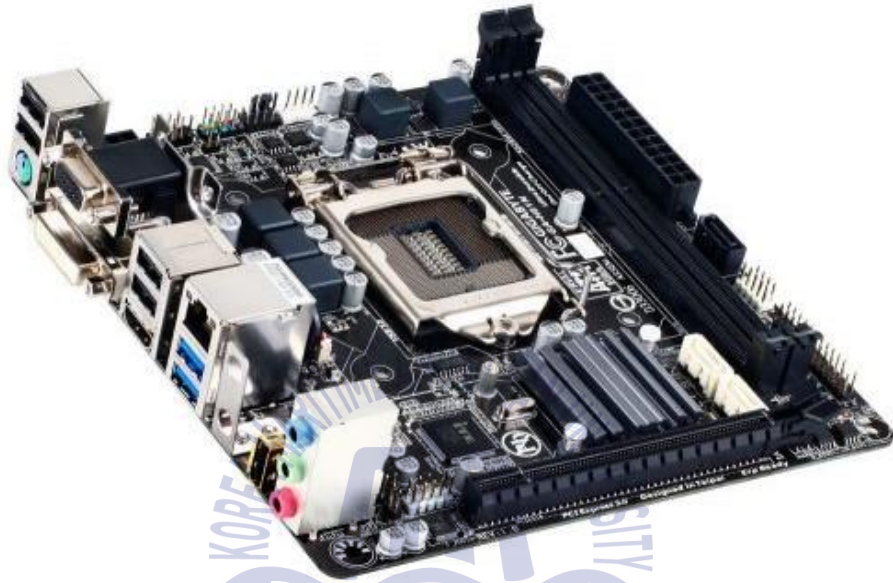


Fig. 4.1 On board PC, mini ITX GA-H81N

The PC board shown in **Fig. 4.1** was used as the primary processing unit for the general operations of the AUV including data collection from the sensors, communication with land and for data saving. The mini-ITX model, with the size of 170mm×170mm, was selected for the PC board, because it uses an Intel core i5, 8G of RAM and SSD memory.

The operating program was developed by using NI LabVIEW, with the purpose of enhancing the operator's access convenience and simplifying the communication method with sensors and thrusters.

Edison board



Fig. 4.2 Edison board with breakout board

In order to modularize the navigation system and apply it to the AUV, An Edison board in **Fig. 4.2** was used as a separate processing unit. The Edison module from Intel is composed of an Intel Atom 500MHz dual core, dual thread CPU, 1GB of RAM and 4GB flash memory as a SoC which uses Intel's Quark 100MHz micro controller. Also, for convenience, it provides Wifi and Bluetooth communications. Also, the board can be expanded for a safe power supply and USB communications. Maximum size is 61mm×29mm×12mm.

Yocto Linux was installed in the Edison board and navigation system module was developed by applying the navigation algorithm based on the Yocto Linux. TCM, DVL, GPS and AHRS are connected to the navigation system module. The calculation results of the navigation system will be delivered to the operating program of the PC through USB communications.

4.1.3 Sensors

GPS

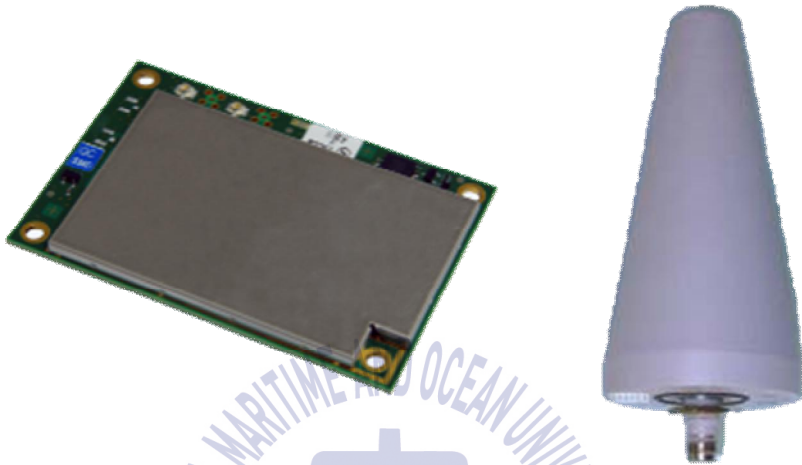


Fig. 4.3 GPS receiver and antenna

The GPS receiver and antenna mounted on the AUV are shown in **Fig. 4.3**. The GPS receiver on the left is an Asterx-M OEM board from Septentrio whose size and weight are 70mm×47.5mm and 47g respectively. The GPS antenna on the right is a spiral antenna from Antcom and a FKM model was used for the water tight of AUV. The antenna's diameter is 66mm and the height is 133mm.

The receiver is installed in extended boards with separate connectors including the SMA and USB ports. It is connected to the PC by USB to supply power and conduct data communications. Also, it transmits data to the antenna through a SMA-TMC cable.

The noise characteristics of the GPS positional data were checked by conducting a separate sensor test on land. The output frequency of the measurements was set to 10Hz through Rxttools provided by Septentrio.

DVL



Fig. 4.4 Doppler velocity logger

The NavQuest 600 Micro of LinkQuest shown in **Fig. 4.4** was installed in the AUV in order to measure the velocity of the AUV. The sensor measures velocity by receiving reflected acoustic signals and it has 4 bulging transducers for transmitting an acoustic beam with a 22° beam. The measured values will be delivered to the Edison board through serial communication. The detailed dimensions and specifications of the installed DVL are shown in **Table 4.2**.

Table 4.2 DVL, NavQuest 600 Micro specifications

Parameter	Specification	Parameter	Specification
Frequency	600 kHz	Maximum transmit	80 watts
Accuracy	1% ± 1 mm/s	Receiver	1.2 watts
Maximum altitude	110 m	Input voltage	24 ± 2 V
Minimum altitude	0.3 m	Transducer assembly diameter	12.6 cm
Maximum velocity	± 20 knots	Housing diameter	17 cm
Standard depth	800 m	Overall length	17 cm
Weight in air	2.9 kg	Weight in water	1.2 kg

TCM



Fig. 4.5 Tilt-compensated compass module

The TCM3 shown in **Fig. 4.5** was used to measure the attitude of the AUV. Its detailed dimensions and specifications are shown in **Table 4.3**.

Table 4.3 Magnetic compass, TCM3 specifications

Parameter	Specification
Dimension (L×W×H)	35mm×43mm×13mm
Weight	< 7 g
Supply voltage	3.8 to 5 V
Current draw (at maximum sample rate)	20 mA
Accuracy (with < 65°of tilt)	0.5°
Resolution	0.1°
Repeatability	0.05°
Maximum dip angle	85°
Maximum sample rate	30 samples/sec
Operating temperature	-40°C to 85°C

AHRS



Fig. 4.6 Attitude and heading reference system

The MTi AHRS of XSENS shown in **Fig. 4.6** was installed in order to measure the angular velocity r for Z_0 axis of the AUV. Its detailed dimensions and specifications are shown in **Table 4.4**.

Table 4.4 MTi AHRS specifications

Parameter	Specification
Dimension (L×W×H)	58mm×58mm×22mm
Weight	50 g
Supply voltage	5 V
Power consumption	350 mW
Static accuracy (roll/pitch)	0.5°
Static accuracy (heading)	1°
Dynamic accuracy	2° RMS
Resolution	0.05°
Repeatability	0.2°
Maximum update rate	256 Hz
Operating temperature	-40°C to 85°C

Pressure sensor



Fig. 4.7 Pressure sensor

The pressure sensor used to measure the depth of the AUV is a PSC and is shown in **Fig. 4.7**. The study used a PSC which has the output terminal form of a DIN 43650-A connector shown in **Fig. 4.8**.

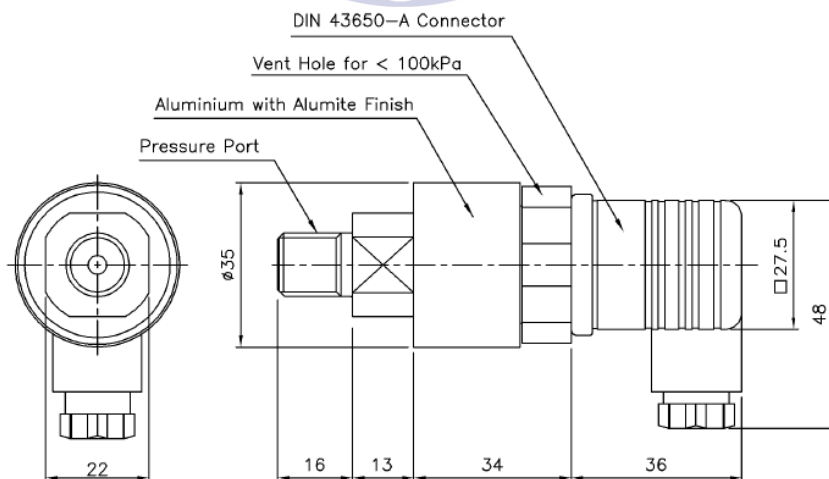


Fig. 4.8 DIN 43650-A connector type



Fig. 4.9 NI USB-6009 DAQ board

The sensor measures pressure within the range of 0.5bar and has an analog voltage output of 1~5V accordingly. Hence, the output could be measured, by using NI USB-6009 that is one of the Data Acquisition (DAQ) device and is shown in **Fig. 4.9**. USB-6009 was powered with a USB and was small enough to be portable. It is a multi functional DAQ board which provides 8 analog inputs with 14bit resolution, two analog outputs with 12bit resolution and 12 digital inputs and outputs. The board's length is 85.1mm and width is 81.8mm and the height is 23.1mm.

The additional specifications for the analog inputs used in the test had the maximum voltage range of -10~10V and accuracy of 7.73mV.

4.1.4 Thrusters



Fig. 4.10 Tecnydyne model 280 and 300

The hovering-type AUV used two horizontal thrusters and two vertical thrusters to perform 4-DOF movement. Tecnydyne model 280 and 300 shown in **Fig. 4.10** were used for the vertical and horizontal thrusters respectively. The detailed specifications for the thrusters are shown in **Table 4.5**.

Table 4.5 Thruster specifications

Parameter	Specification	
	model 280	model 300
Weight	0.9 ~ 1.3 kg (in air) 0.8 ~ 1.3 kg (in water)	1 ~ 1.4 kg (in air) 0.8 ~ 1.3 kg (in water)
Control voltage	-5 ~ +5 V	-5 ~ +5 V
Input voltage	24 Vdc	24 Vdc
Bollard output	6.1 kgf (in both forward & reverse)	7.7 kgf (in forward) 3.2 kgf (in reverse)
Depth rating	850 m	850 m

The forward and backward propulsion force of the thrusters are controlled by analog voltage of $-5\sim 5V$. The analog voltage was generated by using a NI cDAQ-9264 as shown in **Fig. 4.11**. The cDAQ-9264 provides 16 analog outputs which have 16bit resolution with a maximum output range of $-10\sim 10V$ and an accuracy of $0.01025V$. The length is $70.68mm$ and the width is $88.11mm$ respectively.



Fig. 4.11 NI cDAQ-9264 DAQ board

4.2 Operating system

The operating system of the hovering-type AUV can be generally classified into a measurement system, a navigation system, a display system and a control system. The block diagram of the operating system is shown in **Fig. 4.12**.

The measurement system is for extracting the necessary data by receiving the measurements of the sensors installed in the AUV and is composed of GPS,

DVL, TCM3, AHRS and a pressure sensor. The measurement system is composed of several modules developed by implementing the hardware and software respectively to receive and process the data of each sensor.

The navigation system was implemented by using C/C++ in the Linux environment. The navigation system receives the necessary data from the measurement system. After that, it obtains the AUV's position and attitude through dead reckoning or the GPS-aided navigation algorithm proposed in this study. The data is saved in the navigation system for the user to debug the navigation system.

The display system was implemented by using NI LabVIEW in the PC. The display system receives information for the operation of the AUV from the measurement system and the navigation system. For convenience, command buttons were made in order to let the operator control the navigation system during the test. The information related to the behavior of the AUV was saved to review the test results and verify the performance of the navigation algorithm. The control system receives the necessary information to let the AUV move following given scenario.

The control system was implemented by designing PD controllers for the two horizontal thrusters and two vertical thrusters in order to control the AUV with the desired heading angle and depth according the scenario set by the operator. The gain of the controller was determined by various tests.

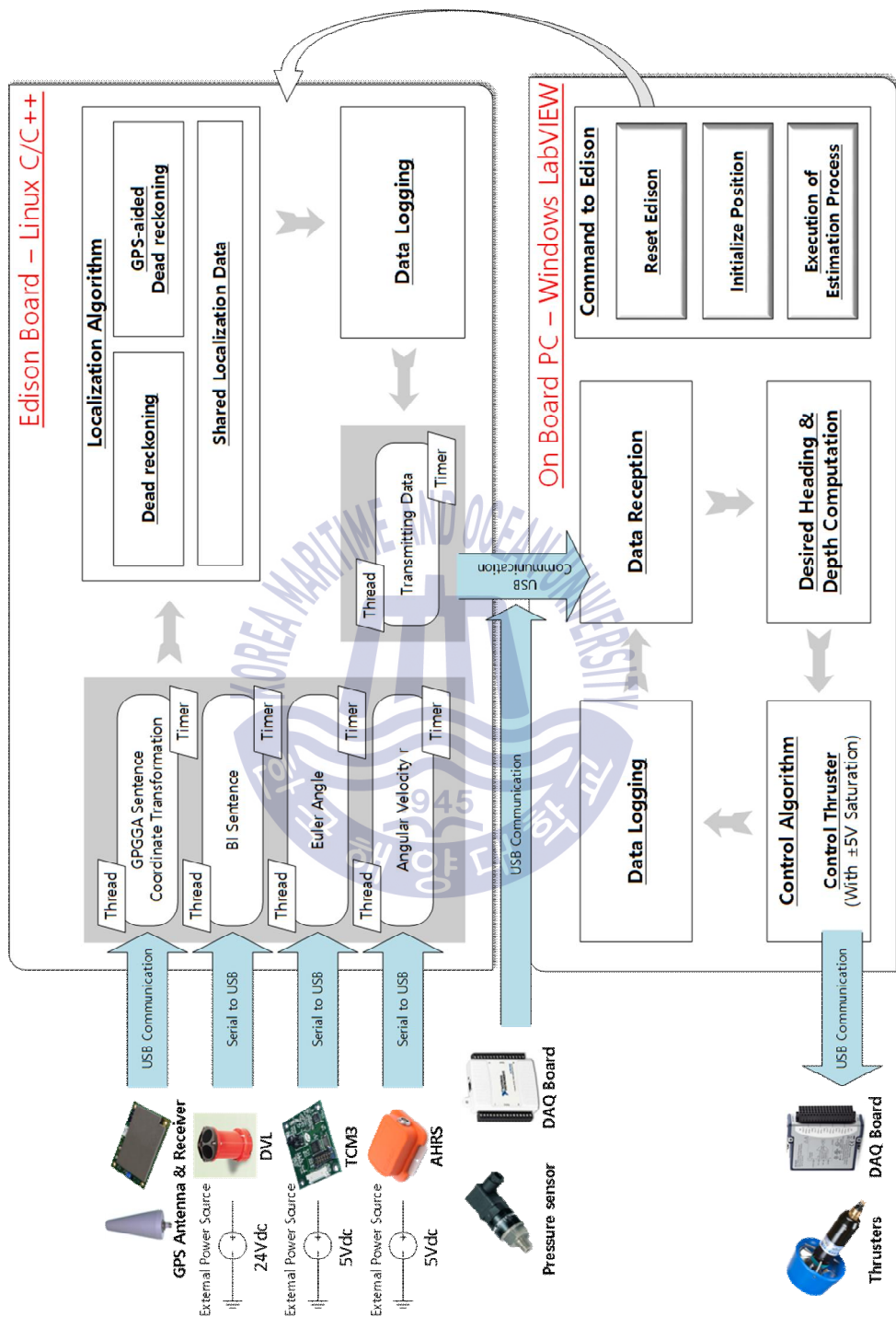


Fig. 4.12 Operating system block diagram

4.3 Experimental overview

A Field test was conducted in order to verify the performance of the GPS-aided navigation algorithm proposed on this study. Since the navigation algorithm uses GPS as an auxiliary sensor, the navigation algorithm shows outstanding performance when the AUV moves in a certain direction on the water. Accordingly, a test scenario, which involves moving in a certain angle through heading control, was implemented in the field test of this study. The performance of the navigation algorithm is verified by checking the estimation performance of the position of AUV and heading bias error for geodetic north through the field test and comparing the position error at the end point.

The heading control test was conducted in real sea where is at the inner harbor of KMOU, located in Yeongdo-gu, Busan, at an average depth of 5m. The test was made to follow the desired depth of 0m and desired heading angle of 0° for 60 seconds. During the test, the status for receiving GPS positional data was outstanding with Horizontal Dilution Of Precision (HDOP) of 1.2 and connected satellites of 8~9.

4.4 Field test results

The heading control test was conducted by moving the AUV on the water throughout all the areas following the desired depth of 0m and a desired heading angle of 0° . The trajectory of the AUV moved on a two-dimensional surface in this test is shown in **Fig. 4.13**. The navigation algorithm estimated the position of the AUV expressed in green ‘•’ by receiving the GPS positional data expressed in magenta ‘+’. Meanwhile, dead reckoning, which does not consider the heading bias error of TCM for geodetic north, can be

seen drawing a biased trajectory towards certain directions shown in the trajectory expressed by the blue line.

The navigation system was developed to estimate the AUV's position and attitude and the TCM's heading bias error, by using the GPS positional data. In this study, the GPS positional data becomes efficient, when the GPS receiving status is in good condition and when the AUV moves fast enough, because of the nondirectional noise characteristics of GPS positional data and the effectiveness of the navigation algorithm.

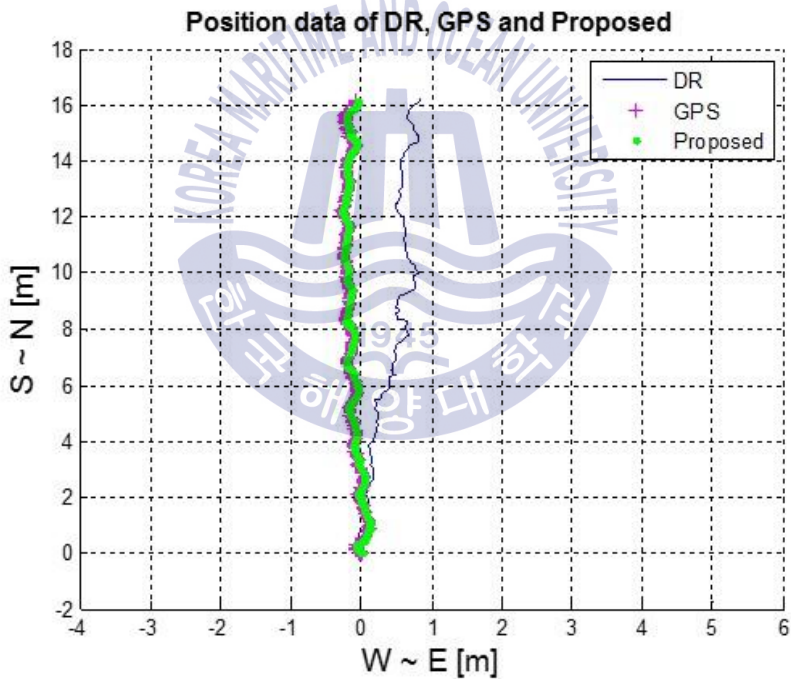


Fig. 4.13 Hovering-type AUV trajectory

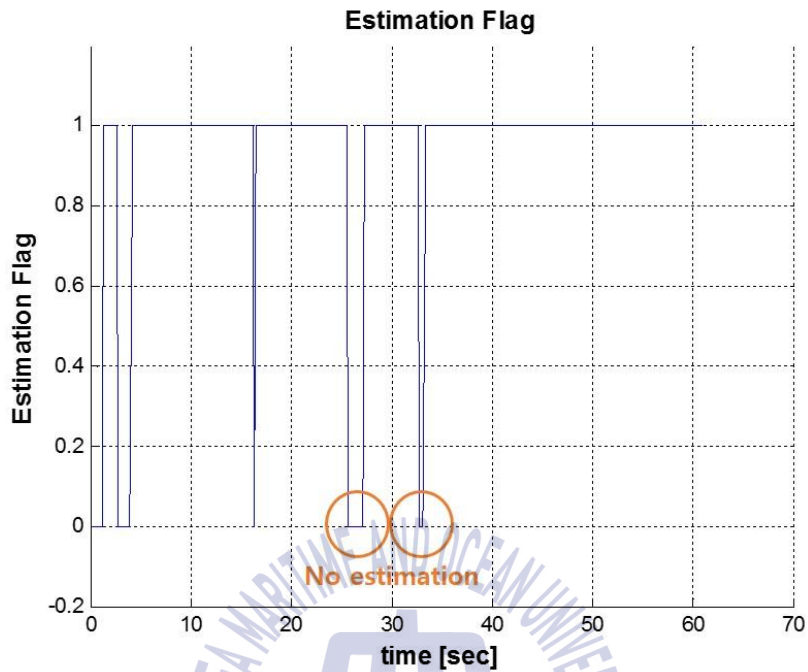


Fig. 4.14 The flag indicating whether to perform the algorithm

The graph shown in **Fig. 4.14** represents the validity of conducting the proposed navigation algorithm. The number 1 in the graph shows that the use of the navigation algorithm was effective and it estimated the position of the AUV and the TCM's heading bias error for geodetic north by using GPS positional data. Meanwhile, the number 0 shows that the position of the AUV was estimated by dead reckoning and the TCM's heading bias error was not estimated.

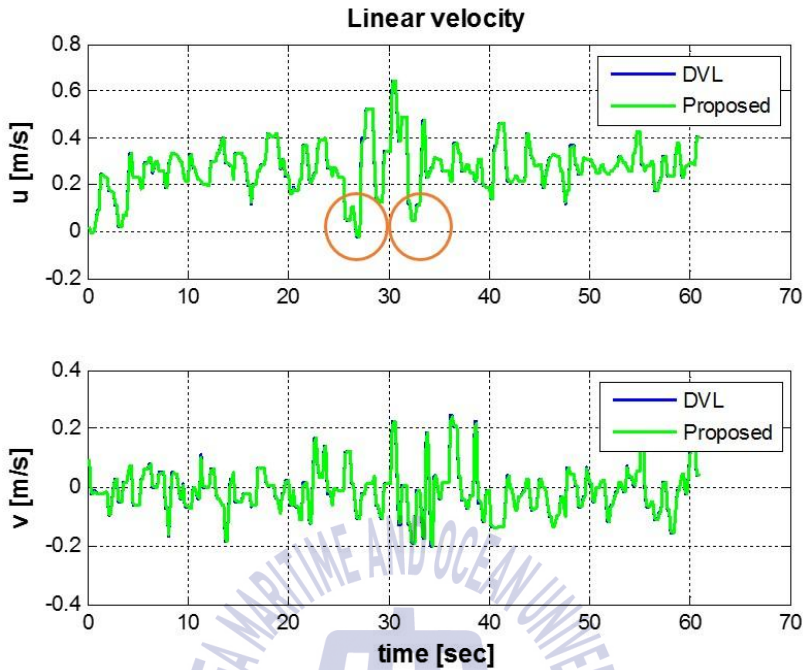


Fig. 4.15 Hovering-type AUV linear velocity

Fig. 4.15 shows the linear velocity of the AUV for X_o axis and Y_o axis. By looking at the two sections of 25~27 seconds and 32~33 seconds in **Fig. 4.14** and **Fig. 4.15**, the navigation algorithm was not performed because the surge velocity u grew less.

Fig. 4.16 shows the TCM's heading bias error estimated by the navigation algorithm. It can be also confirmed that the navigation algorithm uses the last estimated heading bias error in those sections.

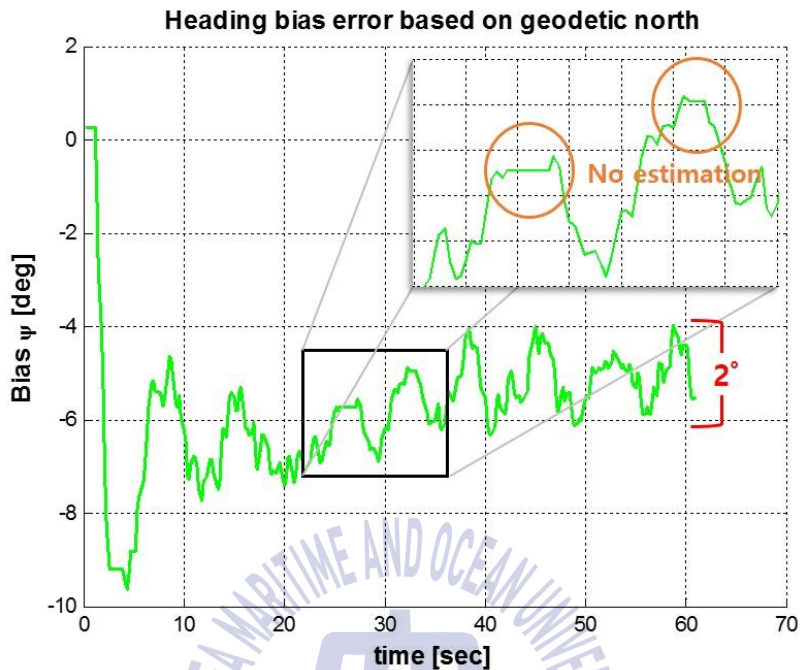


Fig. 4.16 The estimated heading bias error of TCM

The estimated heading bias error of the TCM based on geodetic north was converged within 2° of $-4^\circ \sim -6^\circ$. The magnetic declination of -7.79° was calculated in National Centers for Environmental Information (NCEI) of the US National Oceanic and Atmospheric Administration (NOAA) on the basis of the test date and location (NCEI of NOAA). It can be seen that it similarly estimated the magnetic declination of -7.79° , considering the torsion angle b_ψ^{mount} of the TCM based on a body-fixed coordinate system.

Fig. 4.17 expresses the desired heading angle of the heading control test and the measurements of the TCM and the estimated heading angle of the navigation algorithm.

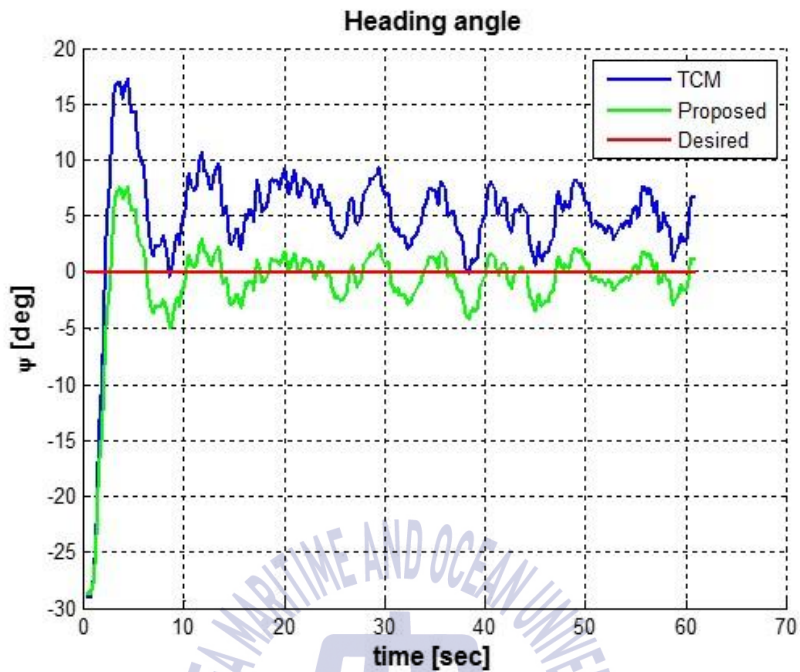


Fig. 4.17 Hovering-type AUV heading angle

The desired heading angle of 0° is shown in the red line and the heading angle measured by the TCM is shown in the blue line. Considering the TCM's heading bias error, the navigation algorithm estimated the heading angle ψ based on the geodetic north and it is shown in the green line. It can be seen that the TCM measurements and the desired heading angle show some differences, because the navigation algorithm estimates the heading bias error.

The distance the AUV traveled was based on the X axis (south to north) and Y axis (west to east) of **Fig. 4.13** and is expressed in **Fig. 4.18**.

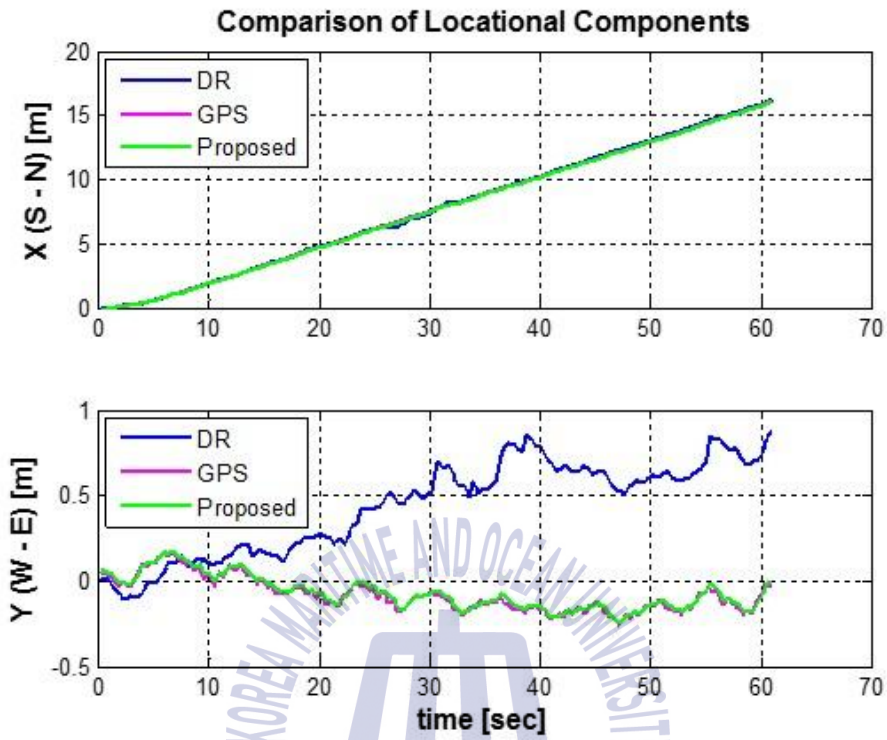


Fig. 4.18 X and Y axis distance traveled

The travel distance for each axis obtained by the GPS positional data is shown in the magenta line. The position estimated by the navigation algorithm is shown in the green line. Meanwhile, the travel distance for each axis of the AUV using dead reckoning, which did not consider the TCM's heading bias error, is shown in the blue line.

Table 4.6 shows the GPS positional data as a reference value and compares the end point position by axis.

Table 4.6 End point position and distance comparisons

Axis	GPS	Dead reckoning		GPS-aided navigation algorithm	
	Position	Position	Distance	Position	Distance
X	16.17 m	16.26 m	0.09 m	16.14 m	0.03 m
Y	-0.03 m	0.865 m	0.895 m	-0.01 m	0.02 m

Dead reckoning which did not consider the TCM's heading bias error showed a 0.9m position error at the end point when the AUV traveled 16m for 60 seconds. It was accumulated proportionally to the travel time and the distance traveled. And, a improved position error of 0.036m was seen at the end point. When using the navigation algorithm, the estimation performance of the AUV's position was considerably improved in comparison to dead reckoning despite the longer travel time and distance. Moreover, even when the algorithm was not performing for various reasons, it was confirmed that the position errors did not accumulate since it considered the last estimated value of the TCM's heading bias error. The results of field test verified the performance of the proposed GPS-aided navigation algorithm.

CHAPTER 5 CONCLUSION

This study proposed the GPS-aided navigation algorithm of the AUV using an extended Kalman filter. In order to verify the performance of the navigation algorithm, a dynamic simulation was conducted by implementing a dynamic simulation program and a heading control test was conducted in a real sea environment. The navigation algorithm is the combined navigation of dead reckoning and satellite navigation. It was designed by using an extended Kalman filter which has less computational complexity compared to unscented Kalman filter or particle filter.

The navigation algorithm receives the GPS positional data when the AUV surfaced, improves the accumulated position error of dead reckoning, which uses DVL and magnetic compass, and estimates the magnetic compass' heading bias error. By reconciling the coordinate system of dead reckoning to the satellite coordinate system considering the magnetic compass' heading bias error including magnetic declination, the position error caused by discordance with reference coordinate system was improved.

The dynamic simulation program was implemented by using the NPS ARIES AUV model and applying the navigation algorithm. By deciding the elements of error covariance of navigation algorithm and generating the measurements for each sensor considering the characteristics of sensors actually being used, the results of the dynamic simulation can be compared/analyzed/referred when verifying performance of the navigation algorithm through field test using a hovering-type AUV.

Two way-point control simulations and a heading control simulation were conducted by using the dynamic simulation program. The performance of the navigation algorithm was verified by improving the accumulated position error of dead reckoning and the position errors caused by discordance with the reference coordinate system.

In order to verify the performance of the GPS-aided navigation algorithm through field test, the navigation system with the navigation algorithm was developed and it was implemented in the hovering-type AUV. The performance of estimating the position of the AUV and estimating the TCM's heading bias error was verified by conducting a heading control test. The performance of the navigation algorithm was also verified by comparing the end point position estimated by the navigation algorithm and dead reckoning.

When applying the GPS-aided navigation algorithm with a UUV as proposed in this study, it is necessary to adjust the covariance matrix of the navigation algorithm by considering the sensors' noise characteristics. Furthermore, contemplation for effective use of the navigation algorithm considering the dynamic characteristics depending on the platform is likely to be needed. This navigation algorithm will be a great contributor to UUV navigation especially when an UUV is operated for a long time and travels long distances, which causes position errors to accumulate, or when it is difficult to obtain positional data through an acoustic beacon or submarine topography map.

References

- [1] Duane Thompson, David Caress, Charles Paull, David Clague, Hans Thomas and Doug Conlin, 2012, “MBARI mapping AUV operations: In the Gulf of California”, OCEANS’12 MTS/IEEE, Virginia, pp. 1-5.
- [2] D. Thompson, D. Caress, H. Thomas and D. Conlin, 2015, “MBARI mapping AUV operations in the gulf of California 2015”, OCEANS’15 MTS/IEEE, Washington, pp. 1-7.
- [3] T. Brown, J. Damiano, S. Jhala, R. Moore, B. Morgan, V. Nguyen, T. Opheim, T. Ringwald, W. Roman, and J. Turk, 2012, Next generation mine countermeasures for the very shallow water zone in support of amphibious operations, Naval Postgraduate School, Monterey, California, No. NPS-SE-12-001, pp. 1-401.
- [4] 대양전기공업, 2003, 무인잠수정의 운항제어 및 매니플레이터 기술개발, 00-D-R-03 -01.
- [5] Bong-huan Jun, et al., 2007, “Development and tank test of an autonomous underwater vehicle ‘ISiMI’”, Journal of Ocean Engineering and Technology, Vol. 21, No. 2, pp. 67-74.
- [6] Jae-weon Choi, Tae-kyu Ha, Binugroho Eko Henfri, Chang-ho Yu and Young-bong Seo, 2010, “Design of a Test bed and Performance Evaluation for a hovering-type Autonomous Underwater Vehicle under Open Control Platform”, Journal of Institute of Control, Robotics and Systems, Vol. 16, No. 5, pp. 489-497.
- [7] Sung-min Hong, 2015, “A study on autonomous navigation system for hovering-type AUV”, Thesis of Korea Maritime and Ocean University, Busan.
- [8] Sung-hyub Ko, Dong-hee Kim and Joon-young Kim, 2013, “Implementation and field test for autonomous navigation of manta UUV”, Journal of the Korean

Society of Marine Engineering, Vol. 37, No. 6, pp. 644-652.

- [9] Joo-no Sur, 2010, 수중로봇 실용화 방안 연구, The Korean Society of Ocean Engineers.
- [10] Liam Paull, Sajad Saeedi, Mae Seto and Howard Li, 2014, "AUV Navigation and Localization: A Review", IEEE Journal of Oceanic Engineering, Vol. 39, No. 1, pp. 131-149.
- [11] E.R. Bachmann, I. Duman, U.Y. Usta, R.B. McGhee, X.P. Yun and M.J. Zyda, 1999, "Orientation Tracking for Humans and Robots Using Inertial Sensors", Proc. of 1999 Symposium on Computational Intelligence in Robotics & Automation, Monterey, CA.
- [12] Joao Luis Marins, Xiaoping Yun, Eric R. Bachmann, Robert B. McGhee and Michael J. Zyda, 2001, "An Extended Kalman Filter for Quaternion-Based Orientation Estimation Using MARG Sensors", Proc. 2001 IEEE/RSJ International Conference on Intelligent Robots and Systems, pp. 2003-2011.
- [13] Seok-ki Jeong, Hyun-taek Choi and Nak-yong Ko, 2014, "Comparison of Attitude Estimation Methods for DVL Navigation of a UUV", Journal of Korea Robotics Society, Vol. 9, No. 4, pp. 216-224.
- [14] Chong-moo Lee, Pan-mook Lee and Woo-jae Seong, 2003, "Underwater hybrid navigation algorithm based on an inertial sensor and a doppler velocity log using an indirect feedback Kalman filter", Journal of Ocean Engineering and Technology, Vol. 17, No. 6, pp. 83-90.
- [15] Kyung-soo Lee and Hee-byung Yoon, 2011, "Improvement of position estimation based on the multisensor fusion in underwater unmanned vehicles", Journal of Korean Institute of Intelligent Systems, Vol. 21, No. 2, pp. 178-185.
- [16] Tae-suk Yoo and Seon-il Yoon, 2013, "DVL-RPM based velocity filter design for a performance improvement underwater integrated navigation system", Journal of Institute of Control, Robotics and Systems, Vol. 19, No. 9, pp. 774-781.
- [17] M. Karimi, M. Bozorg and A.R. Khayatian, 2013, "A comparison of DVL/INS fusion by UKF and EKF to localize an autonomous underwater vehicle", Proc. of the 2013 RSI/ISM International Conference on Robotics and Mechatronics,

pp. 62-67.

- [18] Grace Jean, 2015, USN outlines way ahead for large displacement UUV, IHS Jane's Defence Weekly, US, 22, Oct.
- [19] Jong-hwan Lim and Chul-ung Kang, 2004, "3-D localization of an autonomous underwater vehicle using extended Kalman filter", Journal of the Korean Society of Precision Engineering, Vol. 21, No. 7, pp. 130-135.
- [20] Won-suck Choi, Nhat-minh Hoang, Jae-hoon Jung and Jang-myung Lee, 2014. "Navigation system development of the underwater vehicles using the GPS/INS sensor fusion", 7th International Conference of Intelligent Robotics and Applications, pp. 491-497.
- [21] Young-sik Park, Dong-hyuk Lee, Won-suck Choi and Jang-myung Lee, 2015, "Sea-surface localization of AUV using extended Kalman filter for INS/GPS", in Conference of Institute of Control, Robotics and Systems, Daejeon, Korea, pp. 97-98.
- [22] Thor I. Fossen, 2011, Handbook of marine craft hydrodynamics and motion control, JOHN WILEY & SONS, Chichester, United Kingdom.
- [23] The Society of Naval Architects and Marine Engineers (SNAME), 1950. Nomenclature for Treating the Motion of a Submerged Body Through a Fluid. Technical and Research Bulletin, No. 1-5.
- [24] Thor I. Fossen, 1994, Guidance and Control of Ocean Vehicles, JOHN WILEY & SONS, Chichester, United Kingdom.
- [25] Anthony J. Healey and David Lienard, 1993, "Multivariable sliding mode control for autonomous diving and steering of unmanned underwater vehicles", IEEE Journal of Oceanic Engineering, Vol 18, No 3, pp. 327-339.
- [26] M. Gertler and G.R. Hagen, 1967. Standard Equations of Motion for Submarine Simulations. NSRDC Report 2510.
- [27] Richard J. Boncal, 1987, "A study of model based maneuvering controls for autonomous underwater vehicles", Thesis of Naval Postgraduate School, Monterey, California.
- [28] N.S. Smith, J.W. Crane and D.C. Summey, 1978, SDV Simulator Hydrodynamic Coefficients, NCSC Technical Memorandum, 231(78).
- [29] Dong-ho Choi, Young-jin Lee, Sung-min Hong and Joon-young Kim, 2016,

“Development of hovering-type AUV test-bed ‘OCTAGON’”, Journal of the Korean Society of Marine Engineering, Vol. 40, No. 6, pp. 516-526.

- [30] National Centers for Environmental Information (NCEI) of National Oceanic and Atmospheric Administration (NOAA). Magnetic field calculators [internet]. Available: <https://www.ngdc.noaa.gov/geomag-web/#declination>



Acknowledgement

